

## Original Article

**Cite this article:** Khare SP, Madhok A, Patta I, Sukla KK, Wagh VV, Kunte PS, Raut D, Bhat D, Kumaran K, Fall C, Tatu U, Chandak GR, Yajnik CS, and Galande S. Differential expression of genes influencing mitotic processes in cord blood mononuclear cells after a pre-conceptional micronutrient-based randomised controlled trial: Pune Rural Intervention in Young Adolescents (PRIYA). *Journal of Developmental Origins of Health and Disease* doi: [10.1017/S204017442200068X](https://doi.org/10.1017/S204017442200068X)

Received: 30 June 2022  
Revised: 14 November 2022  
Accepted: 2 December 2022

### Keywords:





Vitamin B12 and micronutrients; randomised controlled trial; cord blood mononuclear cells; gene expression profiling; cell cycle; mitotic processes

### Address for correspondence:

Chittaranjan S. Yajnik, Diabetes Unit, King Edward Memorial Hospital and Research Centre, Pune, India.  
Email: [csyajnik@gmail.com](mailto:csyajnik@gmail.com);  
Sanjeev Galande, Centre of Excellence in Epigenetics, Department of Biology, Indian Institute of Science Education and Research (IISER), Pune, India.  
Email: [sanjeev@iiserpune.ac.in](mailto:sanjeev@iiserpune.ac.in)

Satyajeet P. Khare and Ayush Madhok contributed equally.

# Differential expression of genes influencing mitotic processes in cord blood mononuclear cells after a pre-conceptional micronutrient-based randomised controlled trial: Pune Rural Intervention in Young Adolescents (PRIYA)

Satyajeet P. Khare<sup>1,2</sup> , Ayush Madhok<sup>1</sup>, Indumathi Patta<sup>1</sup>, Krishna K. Sukla<sup>3</sup>, Vipul V. Wagh<sup>2</sup>, Pooja S. Kunte<sup>3</sup>, Deepa Raut<sup>3</sup>, Dattatray Bhat<sup>3</sup>, Kalyanaraman Kumaran<sup>4</sup> , Caroline Fall<sup>4</sup>, Utpal Tatu<sup>5</sup>, Giriraj R. Chandak<sup>6</sup>, Chittaranjan S. Yajnik<sup>3</sup>  and Sanjeev Galande<sup>1,7</sup> 

<sup>1</sup>Centre of Excellence in Epigenetics, Department of Biology, Indian Institute of Science Education and Research (IISER), Pune, India; <sup>2</sup>Symbiosis School of Biological Sciences (SSBS), Symbiosis International (Deemed University), Lavale, Pune, India; <sup>3</sup>Diabetes Unit, King Edward Memorial Hospital and Research Centre, Pune, India; <sup>4</sup>Medical Research Council Lifecourse Epidemiology Centre, Southampton, UK; <sup>5</sup>Indian Institute of Science (IISc), Bangalore, India; <sup>6</sup>Genomic Research on Complex Diseases (GRC-Group), CSIR-Centre for Cellular and Molecular Biology (CSIR-CCMB), Hyderabad, India and <sup>7</sup>Department of Life Sciences, Shiv Nadar University, Gautam Buddha Nagar, Uttar Pradesh, India

## Abstract

In The Pune Maternal Nutrition Study, vitamin B12 deficiency was seen in 65% of pregnant women, folate deficiency was rare. Maternal total homocysteine concentrations were inversely associated with offspring birthweight, and low vitamin B12 and high folate concentrations predicted higher offspring adiposity and insulin resistance. These findings guided a nested pre-conceptional randomised controlled trial 'Pune Rural Intervention in Young Adolescents'. The interventions included: (1) vitamin B12+multi-micronutrients as per the United Nations International Multiple Micronutrient Antenatal Preparation, and proteins (B12+MMN), (2) vitamin B12 (B12 alone), and (3) placebo. Intervention improved maternal pre-conceptional and in-pregnancy micronutrient nutrition. Gene expression analysis in cord blood mononuclear cells in 88 pregnancies revealed 75 differentially expressed genes between the B12+MMN and placebo groups. The enriched biological processes included G2/M phase transition, chromosome segregation, and nuclear division. Enriched pathways included, mitotic spindle checkpoint and DNA damage response while enriched human phenotypes were sloping forehead and decreased head circumference. Fructose-bisphosphatase 2 (*FBP2*) and Cell Division Cycle Associated 2 (*CDCA2*) genes were under-expressed in the B12 alone group. The latter, involved in chromosome segregation was under-expressed in both intervention groups. Based on the role of B-complex vitamins in the synthesis of nucleotides and S-adenosyl methionine, and the roles of vitamins A and D on gene expression, we propose that the multi-micronutrient intervention epigenetically affected cell cycle dynamics. Neonates in the B12+MMN group had the highest ponderal index. Follow-up studies will reveal if the intervention and the altered biological processes influence offspring diabetes.

## Introduction

The Developmental Origins of Health and Disease (DOHaD) paradigm proposes that the environment during crucial stages of development modifies gene expression through epigenetic influences which permanently affect the structure and function of the developing organism.<sup>1</sup> This phenomenon is also called 'fetal programming'.<sup>2</sup> This paradigm originated from Prof. David Barker's demonstration that low birth weight (indicative of poor fetal nutrition) was a risk factor for future diabetes and cardiovascular disease.<sup>3</sup> DOHaD theory proposes that improving fetal nutrition will help prevent common non-communicable diseases.

Fetal programming is largely an epigenetic phenomenon and depends on chemical modifications of DNA and histones, or action of microRNAs, all of which influence gene expression.<sup>4</sup> DNA methylation is the most studied mechanism and is influenced by dietary nutrients which provide or generate methyl groups for cellular metabolism.<sup>5,6</sup> These nutrients include vitamins B12, B2, B6, folate, choline, betaine, and proteins.<sup>7</sup> Vitamins A and D are also known to influence gene expression through their interaction with the nuclear receptors.<sup>8,9</sup> Deficiency of these

nutrients in the diet of a pregnant mother manifests in adverse effects on the fetus, including developmental defects (e.g., neural tube defects), growth abnormalities (growth restriction),<sup>10</sup> and are also associated with an increased risk of non-communicable diseases in later life.<sup>11,12</sup>

The Pune Maternal Nutrition Study (PMNS) is a community-based pre-conceptional birth cohort started in 1993 based on Prof. Barker's theory.<sup>13</sup> It was set up in six villages near Pune to study maternal nutritional determinants of fetal growth and to study life-course evolution of the risk of diabetes and related traits in the offspring. We found that two thirds of the pregnant mothers had low vitamin B12 status but folate status was adequate in the majority.<sup>14</sup> Lower maternal folate and higher total homocysteine concentrations were associated with lower offspring birth weight.<sup>13,15</sup> Low maternal vitamin B12 and normal to high folate concentrations were associated with increased risk of diabetes (insulin resistance and adiposity), and low maternal vitamin D status with higher adiposity in the offspring.<sup>14,16</sup> These findings prompted us to set up the Pune Rural Intervention in Young Adolescents (PRIYA) trial.<sup>17</sup> The trial provided vitamin B12 alone or along with other micronutrients (B-complex vitamins, vitamins A, D, and E, and trace elements) and milk proteins to the adolescent women in the PMNS cohort. The long-term aim of this intervention is to reduce diabetes and improve neurocognition in their offspring. In the short term, we aimed to investigate changes in DNA methylome, transcriptome, proteome, and metabolome in the cord blood of the newborn and its birth size. We have recently reported better neurocognitive outcomes in young offspring in the PRIYA trial whose mothers received vitamin B12 alone.<sup>18</sup>

The purpose of this paper is to describe the transcriptomic changes in the cord blood which may provide a mechanistic insight into micronutrient-mediated fetal programming, and possible pathways which may influence long-term outcomes in the offspring.

## Materials and methods

### *The PRIYA trial: ethics permissions and trial registration*

PRIYA is a randomised, double blind, placebo-controlled trial in adolescent participants of the PMNS (Fig. 1). The rationale and methods of the PRIYA trial are described previously.<sup>17</sup> The PRIYA trial was approved by the King Edward Memorial (KEM) Hospital Research Centre Ethics committee and monitored by a Data Safety Monitoring Board and a Scientific Advisory Committee. Informed consent was signed by parents of all participants, and an informed assent was signed by participants below 18 years of age. After attaining 18 years of age, all participants signed their own informed consent. The trial was registered with the CTRI (2012/12/003212) and ISRCTN (32921044).

### *Participants*

Adolescent participants in the PMNS study were screened for vitamin B12 levels and haemoglobin concentrations. Those with severe vitamin B12 deficiency (plasma vitamin B12 concentration <100 pmol/L) or severe anaemia (blood haemoglobin concentration <70 gm/L) were excluded from the trial and treated appropriately. This was to fulfil ethical imperatives of a

placebo-controlled trial. Those with chronic medical conditions were also excluded.

### *Intervention and comparator*

Eligible participants were randomised into three intervention groups: (1) vitamin B12 (2 µg/day) along with multi-micronutrients as per United Nations International Multiple Micronutrient Antenatal Preparation (UNIMMAP),<sup>19</sup> excluding folic acid and conforming to local regulatory requirements (Supplementary Table 1), (2) placebo, and (3) vitamin B12 (2 µg/day) alone. The multi-micronutrient group also received 20 gm of milk powder every day and all three groups received iron and folic acid as per Government of India approved dosage (60 mg elemental iron + 500 µg folic acid once a week before pregnancy and one tablet daily for at least 100 days after diagnosis of pregnancy). Every month, bottles were distributed by local field staff who were in regular touch with the participants. Bottles were returned each month for counting the unused capsules, this information was used for calculating compliance. The trial intervention was continued until delivery of the first live child.

Habitual dietary intake was assessed using food frequency questionnaire, developed, and validated in the PMNS.<sup>13</sup>

### *Outcomes*

A fasting blood sample was obtained for measurement of circulating micronutrients 6–12 months after the intervention was started. Marriages were recorded, and pregnancies were confirmed by a urine pregnancy test. At 28-weeks' gestation women visited KEM Hospital for an obstetric consultation and blood tests (haemogram, micronutrient levels and a fasting 75 g oral glucose tolerance test). In the villages, women consulted local medical practitioners as required. The field staff visited and monitored pregnant women regularly and helped transfer them for delivery at the KEM Hospital, Pune.

Trained research staff attended all deliveries and collected maternal and cord blood samples as per a standardised protocol. An aliquot of cord blood was transferred to PAXgene tubes (BD, USA) and stored at –80°C till processed for extraction of RNA. Details of the delivery were recorded. Detailed anthropometric measurements were made within 24 h of delivery by trained research staff using standardised methods (Supplementary Table 2). Gestational age was calculated from last menstrual period and confirmed by ultrasound measurements, if required.

### *Blood measurements*

Maternal plasma vitamin B12, B6, holo-TC ('active' vitamin B12), folate, and total homocysteine concentrations were measured at screening, 6–12 months after starting intervention, at 28 weeks gestation, and at delivery. Similar measurements were made in the cord blood. Vitamin B2 was measured at all time points except the screening. Supplementary Table 2 describes the laboratory methods used for these measurements.

### *Statistical methods for clinical characteristics*

Maternal and neonatal clinical characteristics are shown as median (5<sup>th</sup>–95<sup>th</sup> centiles). The significance of difference between intervention and placebo groups was tested by Mann–Whitney test.

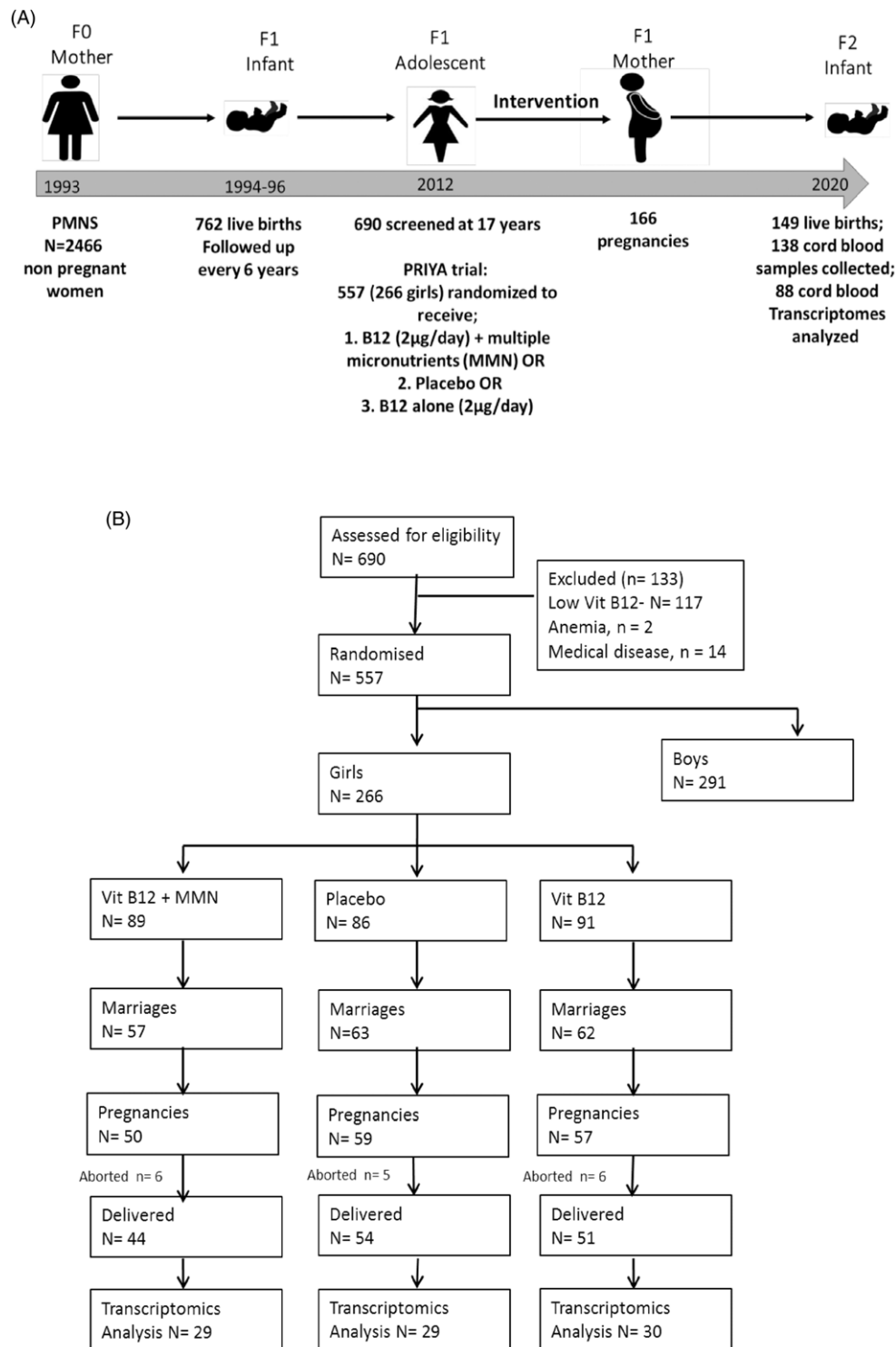


**Fig. 1.** The Pune Maternal Nutrition Study (PMNS) and the Pune Rural Intervention in Young Adolescents (PRIYA) trial. (A) Broad plan of the study. (B) CONSORT diagram of the PRIYA trial.

### Isolation of cord blood mononuclear cells

Mononuclear cells from the cord blood were extracted after depleting RBCs from whole blood. In brief, batches of frozen blood samples were thawed and diluted with one volume of phosphate buffer saline supplemented with EDTA (2 mM). One volume of RBC lysis buffer (Biolegend # 420301) was added to the diluted samples and incubated for 5 min at room temperature. The tubes were

centrifuged at  $350 \times g$  for 15 min at  $4^{\circ}\text{C}$  and the pellets were processed for RNA isolation.

### RNA isolation

Cord blood mononuclear cells were subjected to RNA isolation using TriZol reagent (Invitrogen). Quantitation of RNA was performed on Qubit 4 Fluorometer (Thermo Scientific #Q33238)

**Table 1.** Comparison of maternal characteristics between study participants of three intervention groups

	B12+MMN group: Median (5th, 95th centiles) ( <i>N</i> = 29, 15 boys, 14 girls)	Placebo group: Median (5th, 95th centiles) ( <i>N</i> = 29, 17 boys, 12 girls)	B12 alone group: Median (5th, 95th centiles) ( <i>N</i> = 30, 16 boys, 14 girls)	<i>P</i> -value (B12+MMN vs placebo) (Mann–Whitney U <i>P</i> -value)	<i>P</i> -value (placebo vs B12 alone) (Mann–Whitney U <i>P</i> -value)	<i>P</i> -value (B12+MMN vs B12 alone) (Mann–Whitney U <i>P</i> -value)
<i>Screening</i>						
Age (years)	15.9 (15.6, 17.0)	16.5 (15.6, 16.9)	16.2 (15.6, 16.9)	0.099	0.200	0.802
Haemoglobin (gm/L)	128 (109, 145)	127 (102, 149)	127 (105, 142)	0.474	0.738	0.268
Vitamin B12 (pmol/L)	160.0 (108.0, 273.0)	147.0 (104.4, 238.0)	148.5 (106.0, 272.1)	0.131	0.439	0.544
Holo-TC (pmol/L)	13.0 (6.5, 22.1)	10.1 (5.0, 23.1)	10.2 (5.1, 31.9)	0.096	0.934	0.145
Folate (nmol/L)	15.5 (8.9, 35.7)	21.7 (13.3, 46.2)	17.0 (9.4, 39.3)	<b>0.029</b>	0.117	0.471
Total homocysteine (μmol /L)	21.0 (13.9, 54.5)	24.2 (13.5, 46.1)	22.8 (12.2, 39.1)	0.539	0.328	0.897
<i>Post-intervention (Interim)</i>						
Age (years)	17.3 (16.8, 18.2)	17.7 (16.8, 18.7)	17.5 (16.8, 18.1)	0.184	0.278	0.856
Haemoglobin (gm/L)	120 (106, 133)	120 (99, 136)	117 (91, 130)	1.000	0.219	0.179
Vitamin B12 (pmol/L)	262.0 (108.9, 483.4)	161.9 (107.0, 279.6)	272.5 (165.1, 549.5)	<b>0.000</b>	<b>0.000</b>	0.246
Holo-TC (pmol/L)	23.6 (7.2, 55.9)	8.9 (5.0, 32.4)	28.8 (6.4, 81.3)	<b>0.000</b>	<b>0.000</b>	0.295
Folate (nmol/L)	19.4 (13.5, 38.8)	24.9 (14.6, 69.4)	23.0 (13.0, 55.0)	<b>0.030</b>	0.222	0.375
Total homocysteine (μmol /L)	10.0 (6.7, 24.1)	24.3 (9.9, 49.4)	10.6 (7.6, 19.0)	<b>0.000</b>	<b>0.000</b>	0.850
<i>28 weeks gestation</i>						
Age (years)	21.2 (18.9, 23.9)	21.3 (19.5, 22.9)	21.1 (19.1, 23)	0.578	0.773	0.781
BMI (kg/m <sup>2</sup> )	21.5 (19.1, 27.7)	21.7 (17.4, 31.8)	20.8 (17.8, 26.7)	0.975	0.176	0.080
Haemoglobin (gm/L)	104 (82, 123)	106 (89, 128)	104 (75, 121)	0.635	0.595	0.946
Vitamin B12 (pmol/L)	202.0 (117.8, 606.0)	153.0 (87.0, 424.6)	216.5 (127.1, 506.3)	<b>0.015</b>	<b>0.002</b>	0.135
Holo-TC (pmol/L)	29.4 (11.3, 125.0)	16.6 (7.1, 115.4)	35.3 (10.8, 128.0)	<b>0.009</b>	<b>0.005</b>	0.606
Folate (nmol/L)	42.1 (7.9, 73.9)	45.6 (10.7, 72.6)	48.3 (9.5, 76.7)	0.497	0.85	0.655
Vitamin B2 (pmol/L)	240.0 (171.2, 321.8)	226.0 (164.0, 281.0)	224.0 (156.2, 283.4)	0.351	0.586	0.202
Vitamin B6 (plp) (μg/ml)	4.9 (3.2, 23.6)	3.6 (1.9, 11.5)	3.2 (2.3, 7.3)	<b>0.010</b>	0.720	<b>0.000</b>
Vitamin B6 (pyx) (μg/ml)	1.6 (0.8, 3.6)	1.2 (0.6, 3.4)	1.2 (0.8, 2.1)	0.127	0.913	<b>0.042</b>
Total homocysteine (μmol/L)	6.6 (3.4, 9.1)	6.6 (2.2, 14.9)	6.2 (3.2, 10.8)	0.339	0.252	0.952
<i>At delivery</i>						
Duration of intervention (months)	54.0 (26.4, 78.0)	53.0 (29.6, 77.4)	57.5 (29.5, 77.2)	0.864	0.773	0.879
Compliance (%)	88.8 (66.5, 100.4)	90.8 (67.5, 102.4)	88.9 (68.1, 100.1)	0.524	0.617	0.922

(Continued)

**Table 1.** (Continued)

	B12+MMN group: Median (5th, 95th centiles) (N = 29, 15 boys, 14 girls)	Placebo group: Median (5th, 95th centiles) (N = 29, 17 boys, 12 girls)	B12 alone group: Median (5th, 95th centiles) (N = 30, 16 boys, 14 girls)	P-value (B12+MMN vs placebo) (Mann-Whitney U P-value)	P-value (placebo vs B12 alone) (Mann-Whitney U P-value)	P-value (B12+MMN vs B12 alone) (Mann-Whitney U P-value)
Vitamin B12 (pmol/L)	189.0 (101.2, 504.8)	180.0 (70.6, 376.8)	240.0 (107.2, 448.0)	0.465	<b>0.033</b>	0.135
Holo-TC (pmol/L)	28.1 (7.8, 111.5)	24.6 (9.0, 86.0)	31.2 (10.6, 128.0)	0.312	0.075	0.359
Folate (nmol/L)	30.1 (13.3, 77.2)	43.5 (5.9, 91.3)	33.6 (10.3, 88.5)	0.576	0.805	0.988
Total homocysteine (μmol/L)	7.8 (3.1, 16.3)	8.9 (4.8, 16.2)	8.6 (3.5, 13.8)	0.307	0.324	0.852

IQR: Interquartile range, plp: pyridoxal 5'-phosphate, pyx: pyridoxine; values represent median (IQR); P-values for between group comparison calculated by Mann-Whitney U test and for multi-group comparison by Kruskal Wallis test. P-value is calculated by Kruskal Wallis. Significant P-values (< 0.05) are shown in bold font.

using RNA HS Kit (Thermo Scientific #Q32852). Libraries were prepared according to the manufacturer's protocol (Illumina). Briefly, each sample was run on 2100 Bioanalyzer (Agilent #G2939BA) to check its integrity. About 500 ng of total RNA from each sample was used to make libraries using TruSeq Stranded mRNA Sample Prep Kit (Illumina #20020594). After final quantification and pooling, the libraries were run on Illumina HiSeqX platform, with 150 nucleotides long paired end reads as the output.

### RNA sequencing and data analysis

The quality of sequencing was assessed using FastQC (v0.11.8). The raw sequence reads were aligned to the human genome (hg38, GENCODE)<sup>20</sup> using HiSAT2.<sup>21</sup> The resulting BAM files were used to generate a count matrix using featureCounts for known genes.<sup>22</sup> Samples with reads that aligned poorly (Q1-IQR\*1.5) were excluded from the downstream analysis. Low expression genes (less than 20 counts in total in all samples) were not included for the differential expression analysis. Gene expression levels were normalized by internal normalization method by calculating geometric mean in DESeq2.<sup>23</sup> Normalized expression values were regularized log transformed for principal component analysis (PCA) plots. Differential expression analysis was performed between the placebo group and the intervention groups by two-group comparison using the default Wald test in DESeq2. Maternal age at the start of intervention, duration of intervention, sex of the child, and cord blood monocyte, granulocyte, and lymphocyte counts were used as covariates. Absolute values of these covariates were converted to categorical variables around the median. Since the samples were processed in batches, the batch numbers were also used as a covariate. False Discovery Rate (FDR) adjusted P-value cut-off of 0.05 and base mean value cut-offs of 1 were used for identification of differentially expressed genes (DEGs). Significantly DEGs were subjected to gene enrichment analysis using clusterProfiler (v3.14.3)<sup>24</sup> and gProfiler (version:e105\_eg52\_p16\_e84549f).<sup>25</sup> To understand the gene network, the DEGs were subjected to gene network analysis using STRING.<sup>26</sup>

## Results

### Trial progress and clinical findings

Six hundred and ninety adolescent participants in the PMNS (362 boys, 328 girls) were screened for inclusion in the PRIYA trial in the year 2012 (Fig. 1). A total of 133 were excluded and 557 (266 females, 291 males) were randomised into 3 groups. The intervention was started in September 2012.

This paper refers to outcomes only in female participants. At screening they were ~16 years old, had a median body mass index (BMI) of 18.0 kg/m<sup>2</sup> (56.7% had a BMI <18.5 kg/m<sup>2</sup>), 30.1% were anaemic (haemoglobin <120 gm/L), and average education was 13 years of schooling. This is a predominantly vegetarian population: a third never ate non-vegetarian foods, and a fourth ate it less than once a week. Portion sizes of non-vegetarian foods were very small. Only 30% consumed milk more than alternate days. A total of 182 females married during the trial, 166 became pregnant, and 149 delivered in the study. Cord blood samples were available on 138 for gene expression analysis. This paper reports transcriptome measurements on the first 88 cord blood samples (40 girls, 48 boys); these pregnancies were comparable to the 50 who are not included in this study (for maternal age, BMI, socio-economic status, and haemoglobin concentrations at 28 weeks gestation, *P* > 0.05).

At 28 weeks gestation, the mothers were on average 21 years old and weighed 53.0 kg with a BMI of 22.0 kg/m<sup>2</sup> (Table 1). The first delivery was in November 2014 and the last delivery was in February 2020. The duration of intervention was on an average of 54 months (min = 24, max = 83). Three mothers delivered pre-term, and 23 were delivered by caesarean section. The average birth weight of babies was 2.8 kg, 14 were low birth weight (<2.5 kg) (Table 2). There was no significant difference in the birth weight, length, skin fold thicknesses in the three groups; however, ponderal index was highest in the B12+MMN group. The pregnancy outcomes (pre-term deliveries, caesarean sections, and common adverse events) were similar in the three intervention groups.

At screening, plasma vitamin B12 concentrations were low and 47.7% were vitamin B12 deficient (<150 pmol/L), only 1% were



**Table 2.** Comparison of neonatal characteristics between study participants of three intervention groups

	B12+MMN group: Median (5th, 95th centiles) (N = 29, 15 boys, 14 girls)	Placebo group: Median (5th, 95th centiles) (N = 29, 17 boys, 12 girls)	B12 alone group: Median (5th, 95th centiles) (N = 30, 16 boys, 14 girls)	P-value (B12+MMN vs placebo)	P-value (placebo vs B12 alone)	P-value (B12+MMN vs B12 alone)
<i>Anthropometry</i>						
Birth weight (g)	2951.0 (2151.0, 3560.0)	2760.0 (2276.0, 3584.0)	2778.0 (1790.0, 3323.5)	0.305	0.601	0.083
Birth length (cm)	48.2 (43.9, 52.0)	48.4 (45.6, 50.5)	48.5 (44.8, 51.1)	0.597	0.426	0.850
Ponderal index (g/cm <sup>3</sup> )	2.6 (2.2, 2.9)	2.4 (2.2, 3.0)	2.4 (2.1, 2.7)	<b>0.044</b>	0.791	<b>0.017</b>
Adiposity (sum of skinfolds) (mm)	8.2 (6.2, 10.9)	8.4 (6.1, 13.0)	7.8 (6.0, 11.0)	0.926	0.481	0.490
<i>Cord blood biochemistry</i>						
Vitamin B12 (pmol/L)	292.0 (121.4, 1562.0)	282.0 (118.8, 979.6)	380.5 (94.0, 1752.9)	0.858	0.108	0.154
Holo-TC (pmol/L)	94.7 (15.9, 128.0)	61.3 (23.0, 128.0)	121.7 (24.3, 128.0)	0.634	0.164	0.301
Folate (nmol/L)	47.6 (25.3, 79.0)	56.9 (22.2, 104.8)	55.5 (19.5, 88.5)	0.413	0.671	0.562
Vitamin B2 (pmol/L)	321.0 (214.6, 444.2)	289.0 (222.2, 384.8)	304.0 (227.9, 410.0)	0.401	0.476	0.909
Vitamin B6 (plp) (µg/ml)	32.3 (16.3, 73.9)	23.4 (5.2, 46.7)	23.5 (7.9, 61.6)	<b>0.034</b>	0.622	0.059
Vitamin B6 (pyx) (µg/ml)	5.2 (3.4, 14.5)	4.1 (2.6, 7.4)	4.8 (2.7, 9.4)	<b>0.014</b>	0.154	0.271
Total homocysteine (µmol/L)	6.9 (3.6, 14.3)	7.1 (3, 17.8)	5.6 (3.4, 12.5)	0.602	0.059	0.143
<i>Cord blood haematology</i>						
Haemoglobin (gm/L)	139 (118, 176)	136 (126, 167)	148 (127, 165)	0.774	<b>0.038</b>	<b>0.048</b>
White blood cell count (*10 <sup>3</sup> /uL)	14.2 (10.5, 18.2)	14.9 (10.0, 21.4)	12.9 (8.4, 21.7)	0.719	0.332	0.493
Granulocytes count (*10 <sup>3</sup> /uL)	7.9 (5.1, 11.5)	7.6 (5.2, 12.7)	7.2 (3.7, 12.2)	0.949	0.328	0.455
Lymphocyte (*10 <sup>3</sup> /uL)	5.3 (3.6, 6.8)	5.0 (3.4, 9.1)	5.2 (3.2, 8.9)	0.387	0.666	0.714
Monocyte (*10 <sup>3</sup> /uL)	0.8 (0.2, 2.5)	1.0 (0.3, 1.8)	0.8 (0.4, 2.2)	0.387	0.29	0.944
Red blood cell count (*10 <sup>6</sup> /uL)	4.0 (3.4, 4.8)	3.9 (3.4, 4.7)	4.4 (3.4, 4.8)	0.798	<b>0.008</b>	<b>0.036</b>
Platelet count (*10 <sup>3</sup> /uL)	272.5 (187.4, 348.8)	270.0 (173.2, 384.4)	245.0 (159.9, 339.7)	0.439	0.321	0.054

IQR: Interquartile range, plp: pyridoxal 5'-phosphate, pyx: pyridoxine; values represent median (IQR); P-values for between group comparison calculated by Mann-Whitney U test and for multi-group comparison by Kruskal Wallis test. P-value is calculated by Kruskal Wallis. Significant P-values (< 0.05) are shown in bold font.

folate deficient (<7 nmol/L). Plasma total homocysteine concentrations were high, 91% had hyperhomocysteinaemia (>15 µmol/L). There was no significant difference in plasma vitamin B12, folate, and total homocysteine concentrations in the three

intervention groups. In women, in the two vitamin B12 supplemented groups there was a sizeable rise in vitamin B12 and holo-TC concentrations compared to the placebo group, and a fall in total homocysteine concentrations within a few months

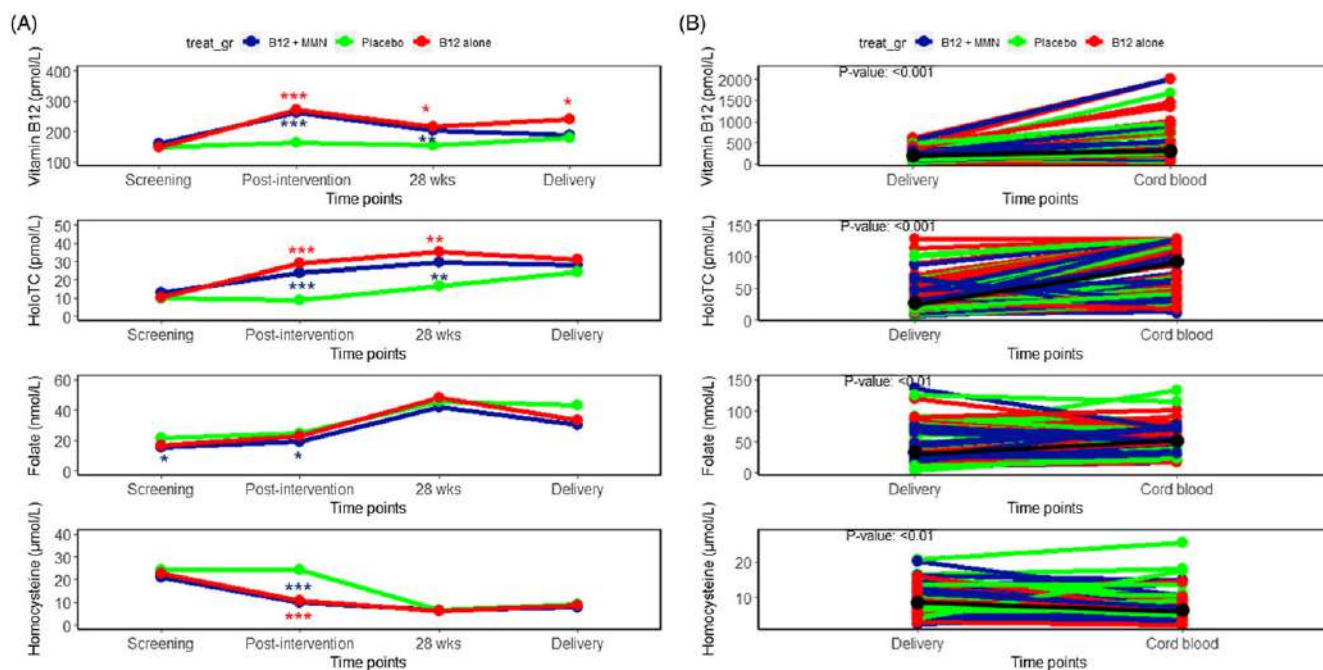


**Fig. 2.** Serial micronutrient levels in the mothers and baby's cord blood in the PRIYA trial. (A) Median concentrations of vitamin B12 (pmol/L), Holo-TC (pmol/L), folate (nmol/L), and total homocysteine (μmol/L) at screening, post-intervention (~6–12 months later), 28 weeks gestation and at delivery in the mothers. (B) Concentrations in the mother at delivery and in the cord blood of the baby are joined for the individual pairs. Concentrations of vitamin B12, holo-TC, and folate were higher and those of total homocysteine lower in the cord blood compared to maternal concentrations at delivery. There was a highly significant association between maternal and cord blood concentrations of these four measurements ( $\rho \sim 0.7$ ,  $P < 0.001$ ). \* $P < 0.05$ , \*\* $P < 0.01$ , \*\*\* $P < 0.001$  denotes significance of difference from the placebo; MMN, multiple micronutrients.

(Fig. 2A). The levels of vitamin B12 and total homocysteine fell during pregnancy (even in the placebo group), but both vitamin B12 and holo-TC remained higher in the two intervention groups. The difference in total homocysteine concentrations between groups was blunted in pregnancy. Vitamins B2 and B6 were the highest in the B12+MMN group at all time points after intervention (Table 1). Maternal haemoglobin concentrations were similar in the three groups throughout the trial. The measured compliance for consumption of intervention capsules was similar in the three intervention groups.

At delivery, compared to placebo, maternal vitamin B12 concentration was higher in the B12 alone group but not in the B12+MMN group. Holo-TC, folate, and total homocysteine concentrations were similar in the three groups (Fig. 2, Table 1). Vitamin B2 and B6 concentrations were highest in the mothers and in the cord blood of B12+MMN group. Maternal concentrations at delivery and cord blood concentrations of vitamin B12 ( $\rho = 0.716$ ,  $P < 0.001$ ), holo-TC ( $\rho = 0.668$ ,  $P < 0.001$ ), folate ( $\rho = 0.711$ ,  $P < 0.001$ ), and total homocysteine ( $\rho = 0.681$ ,  $P < 0.001$ ) were significantly correlated (Fig. 2B). Cord blood haemoglobin concentration and red cell count were highest in the group supplemented with B12 alone. The total leucocyte count and individual counts of granulocytes, lymphocytes, monocytes, and platelets were similar in the three groups.

### RNA sequencing and differential gene expression analysis

Mononuclear cells from 88 cord blood samples were subjected to RNA sequencing. Each sample generated approximately 50 million reads. Out of the 88 samples, 9 samples showed poor alignment against the reference genome and were not considered for the downstream analysis. Our final analysis was therefore, on 79

samples. All samples showed comparable assignment to genes for generation of count matrix. The count matrix was used for differential expression analysis.

Samples showed clear separation based on the sex of the child on PCA, however, no separation was observed based on any other covariate or the intervention (Fig. 3A–3B). Differential expression analysis between the B12+MMN group and placebo resulted in identification of 75 DEGs (Fig. 3C, Table 3, and Supplementary Table 3).

We used clusterProfiler and gProfiler to identify the top biological processes, pathways, and phenotypes affected by the DEGs (Fig. 3D and Supplementary Figure 1). Participants supplemented with B12+MMN showed lower expression of genes associated with mitotic processes such as chromosome segregation, nuclear division, and G2/M phase transition as compared to the placebo group. To understand the gene networking of the 75 DEGs, we performed analysis using STRING. Of the 75 DEGs, 71 formed a network with 12 showing association with the biological process 'negative regulation of cell cycle' (Fig. 3E). Cell proliferation markers such as cyclin D1 (*CCND1*), *PCNA*, and Ki-67 (*MKI67*) did not show significant differences in gene expression; however, pathway analysis identified enrichment of Cell Cycle Checkpoints and DNA damage response pathways. Enrichment of human phenotype terms Sloping forehead and Decreased head circumference was also observed. The 75 genes differentially expressed between B12+MMN and placebo also showed similar trend in expression in the B12 alone group but did not reach statistical significance (Supplementary Table 3). The B12 alone group showed two DEGs [Fructose biphosphatase 2 (*FBP2*) and Cell Division Cycle Associated 2 (*CDCA2*)] compared to placebo of which, *CDCA2* was common to the B12+MMN group (Fig. 3F). No significantly DEGs were observed between the two active intervention groups.

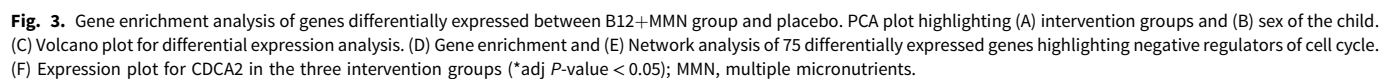




**Table 3.** Top 10 genes that are differentially expressed between placebo and B12+MMN groups

Sr. no.	Gene symbol	B12+MMN vs placebo		B12 alone vs placebo		Chromosomal location
		log2FC	Adj. P-value	log2FC	Adj. P-value	
1	<i>KIF14</i>	−1.248	0.009	−0.731	1	1q32.1
2	<i>KNL1</i>	−1.203	0.009	−0.747	0.93	15q15.1
3	<i>KIF15</i>	−1.114	0.013	−0.562	1	3p21.31
4	<i>DEPDC1</i>	−1.319	0.014	−0.864	0.958	1p31.3
5	<i>TOP2A</i>	−1.085	0.014	−0.56	1	17q21.2
6	<i>CDCA2</i>	−1.206	0.016	−1.197	0.032	8p21.2
7	<i>ESCO2</i>	−1.243	0.016	−0.773	1	8p21.1
8	<i>SKA1</i>	−1.353	0.016	−0.815	1	18q21.1
9	<i>TPX2</i>	−1.073	0.016	−0.729	0.93	20q11.21
10	<i>TRBV7-2</i>	1.02	0.016	0.616	1	7q34

## Discussion

In this communication, we report the effect on the offspring's cord blood transcriptome of a micronutrient intervention in mothers, started before conception (in adolescent age) and continued until the delivery of the child. The PRIYA trial is based in 6 villages near Pune and was guided by findings in the PMNS which showed: (1) a high prevalence of vitamin B12 deficiency in this predominantly vegetarian population,<sup>13,14</sup> (2) that higher maternal total homocysteine concentration during pregnancy was associated with lower offspring birth weight,<sup>15</sup> (3) that low maternal vitamin B12 and normal to high folate status in pregnancy was associated with increased risk of diabetes in the child,<sup>14</sup> and (4) that lower maternal vitamin B12 and folate nutrition was associated with poorer neurocognitive performance in the child.<sup>27</sup> In the PRIYA trial, we supplemented adolescent participants from the PMNS with either vitamin B12 alone or with multi-micronutrients and milk protein, or only placebo. The vitamin B12+MMN intervention resulted in differential expression of 75 genes in the cord blood compared to the placebo group. Vitamin B12 alone influenced the expression of only a few genes, though the pattern of gene expression was similar in the two intervention groups. The DEGs in the B12+MMN group predominantly influenced mitosis related processes such as G2/M phase transition, chromosomal segregation, and nuclear division. B12 alone influenced transcription of *FBP2* and *CDCA2* genes of which *CDCA2* is common to B12+MMN group and involved in chromosomal segregation. To our knowledge, this is the first report of changes in the cord blood transcriptome after a maternal nutritional intervention initiated much prior to conception. Similar studies in the literature have mostly reported changes in DNA methylation in the cord blood but not gene expression. These include, response to maternal vitamin B12 supplementation<sup>28–32</sup> or folic acid supplementation.<sup>33–38</sup> Effects of maternal micronutrient supplements other than vitamin B12 and folate on DNA methylation in the offspring have also been reviewed.<sup>39,40</sup>

Nutritional deficiencies were common in the participants of the PMNS as reflected in low BMI of mothers, relatively low intake of calories, proteins, and micronutrients from a predominantly

vegetarian diet, high prevalence of anaemia, low levels of vitamin B12 and ferritin, and low birth weight of the children.<sup>13,14</sup> The villages were drought-prone, and the population had a low socio-economic status. Our intervention was prompted by our findings in this cohort which are summarised in the previous paragraph. In preparation for this intervention, we investigated and confirmed that absorption of a low dose oral vitamin B12 (2 mcg and 10 mcg) was adequate in this population, thus supporting the thesis that low vitamin B12 status was largely attributable to a low dietary intake.<sup>41</sup> We then performed a 1-year pilot intervention to establish feasibility of a community-based trial and to decide on a dose of vitamin B12 which was physiological and effective in improving one-carbon metabolism.<sup>42</sup> On this background, supplementation in the PRIYA trial achieved a demonstrable increase in circulating concentrations of vitamin B12, holo-TC, B2, and B6 in the B12 + MMN group and of vitamin B12 and holo-TC in the B12 alone group during the pre-conceptional period. The difference from the placebo group persisted in pregnancy even though there was the expected physiological fall in the levels of vitamin B12 and holo-TC. Improved vitamin status resulted in an improvement in maternal one-carbon metabolism, seen in a significant fall in plasma total homocysteine concentrations. In the B12+MMN group, though not measured, we expect an additional improvement in nutrition of vitamins A, D, and E, and other micronutrients (Zn, etc.) given the contents of the UNIMMAP capsules (Supplementary table 1). High folate concentrations in pregnancy are attributable to iron and folic acid supplementation in all 3 groups as per Government of India approved dosage (60 mg elemental iron and 500 µg folic acid daily), thus it was also seen in the placebo group. It is interesting that the concentrations of the vitamins were higher in the cord blood compared to the maternal blood, suggesting active placental transfer. Overall, our intervention translated into better micronutrient nutrition of the ovum before conception and of the conceptus throughout the pregnancy. A relative lack of difference in micronutrient concentrations between intervention and placebo groups in the cord blood may be contributed by altered placental transport, altered binding to carrier proteins, and differential utilisation by the baby.<sup>43,44</sup>

An inspection of the one-carbon metabolic cycle (Fig. 4) and its regulation by B-complex vitamins suggests that mothers and babies who received vitamin B12+MMN would have a more comprehensive effect on nucleotide synthesis, and DNA and RNA metabolism compared to those who received vitamin B12 alone. Higher haemoglobin and red blood cell count in the vitamin B12 alone group may be related to higher levels of vitamin B12 and holo-TC in this group and their specific effect on haemopoietic tissue.

A detailed analysis of the transcriptomic differences suggested that though the overall pattern of differential expression was similar in the two intervention groups, the effect size was greater in the B12+MMN group. Thus, 75 genes were differentially expressed in the B12+MMN group but only two genes (*FBP2* and *CDCA2*) in the B12 alone group. Seventy-one of these 75 DEGs were closely networked and 12 of them showed a negative association with regulation of cell cycle. The affected biological processes included cell cycle G2/M phase transition, chromosome segregation, nuclear division and related. However, a targeted expression analysis of cell proliferation markers such as cyclin D1, Minichromosome Maintenance Complex Component 2 (*MCM2*), Proliferating Cell Nuclear Antigen (*PCNA*) and Ki-67,<sup>44</sup> did not show any significant difference in any of the intervention groups compared to the placebo group. Intriguingly, cell cycle checkpoint and DNA

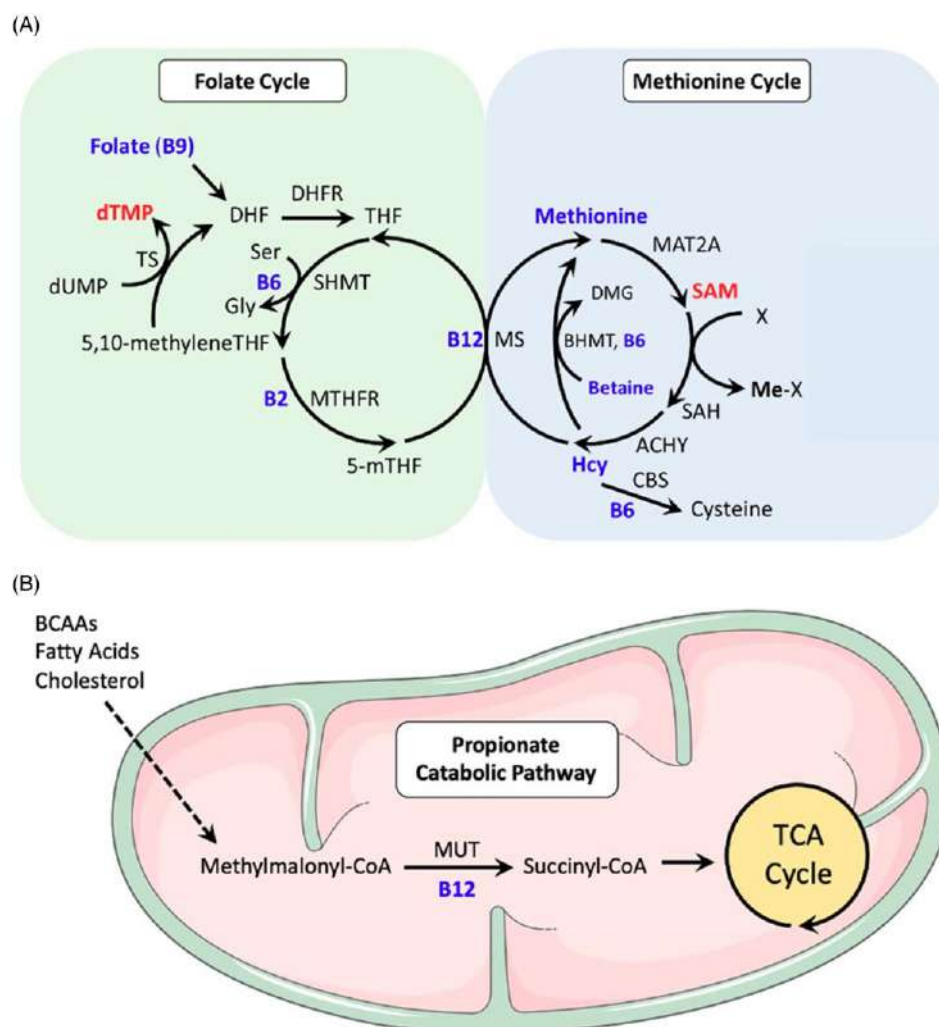


**Fig. 4.** One-Carbon Metabolism and PRIYA trial. (A) One-carbon metabolism is a central metabolic pathway combining folate cycle and methionine cycle. Folate cycle generates nucleotides which help DNA synthesis and repair while methionine cycle generates methionine and S-adenosyl methionine (SAM). Methionine is a component of all cellular proteins and SAM methylates a wide range of cellular molecules including DNA (an epigenetic mechanism), lipids (important in nervous system), and proteins. Folate cycle is influenced by a number of B-complex vitamins (B2, B6, B9 and B12) as is the methionine cycle (B6, B12). Dietary proteins provide the amino acid serine which is the primary donor of methyl groups, and other amino acids which get incorporated in protein molecules. (B) Vitamin B12 has an additional influence on mitochondrial energy metabolism through its action as a cofactor to mutase enzyme which converts methylmalonic acid to succinic acid (adapted from Lyon et al., 2020<sup>53</sup>).

repair related genes showed higher expression in the placebo group.

We propose that low concentrations of micronutrients in the placebo group resulted in hypomethylation of the relevant genes and consequently increased the expression of genes involved in nucleic acid synthesis and cell division. However, micronutrient deficiency compromised the supply of nucleotides for DNA synthesis and replication resulting in activation of cell cycle checkpoint. Thus, genes related to DNA synthesis and cell division appear relatively under-expressed in the B12+MMN group because the intervention led to better micronutrient status influencing methylation status of those relevant genes. Interestingly, in another study of vitamin B12 and/or folic acid supplementation in 9 year old children, we reported differential DNA methylation of genes associated with G2/M checkpoint regulation.<sup>45</sup> The MMN supplementation also included vitamins A and D, and zinc which are known to affect gene expression in specific tissues<sup>46–48</sup> and may have contributed to some of DEGs in the B12+MMN group. A review has summarised the recent exciting understanding of the role of core cellular metabolites (ATP, S-adenosyl methionine, acetyl-CoA, NAD/NADP, and  $\alpha$ -ketoglutarate) in the nuclear compartment to influence the epigenome; all these metabolites are likely to be influenced in our intervention.<sup>49</sup> Association of transcriptomic changes with aspects of facial and head development

is intriguing and it will be of interest to see if they reflect in any phenotypic features during follow up of the children, especially in the neurocognitive domain.

Features of vitamin B12 deficiency are usually described in relation to pernicious anaemia (a genetic-immunologic condition causing absence of 'intrinsic factor' which is essential for vitamin B12 absorption). The biochemical and cellular changes include: block in deoxyuridine to thymidine conversion leading to disturbed DNA synthesis and repair, prolongation of S-phase, maturation arrest (G2/M transition), and failure of cell division.<sup>50</sup> There is a remarkable similarity in these disturbances and our findings. We could not find any reports of transcriptomic alterations in this condition. Two studies investigated the effect of cobalamin deficiency on nerve cells in culture: there was slower proliferation and accelerated differentiation of neuroblastoma cells<sup>51</sup> and impaired DNA synthesis, prolonged G2/M phase transition leading to cell growth without cell division in human astrocytes.<sup>52</sup> Again, no transcriptomic data was available.

### Strengths and Limitations

A major strength of our intervention is that it was guided by past nutritional observations in the same cohort and that it was truly pre-conceptional (from adolescent age). Thus, our trial had the

potential to influence peri-conceptual epigenetic reprogramming. Use of 'physiological' doses of micronutrients was based on the successful results of an absorption study and a pilot trial<sup>42</sup> which made it public health relevant. The limitations include that these preliminary results are on a relatively small number. The limited power could also have contributed to a lack of difference in the cord blood measurements of some of the micronutrients and in body size measurements of the babies in the three groups. Another limitation is that the transcriptomic measurements are limited only to cord blood mononuclear cells which may not reflect changes in other tissues and those earlier in the pregnancy. Such invasive studies are difficult in humans for ethical reasons. It should be noted that the transcriptome analysis using cord blood mononuclear cells acts as a surrogate to gain insights into the multitude of changes in the gene expression profiles resulted due to the in-utero programming following the nutritional intervention.

In conclusion, we provide the first evidence of the influence of human maternal pre-conceptual micronutrient intervention on the gene expression profile of the cord blood at delivery. Supplementation with vitamin B12 and other micronutrients influenced vital cellular processes such as cell cycle regulation, mitotic division, and growth of facial and head structures. These gene expression changes provide plausible mechanisms mediating intrauterine programming of future health and disease. In subsequent papers we intend to report the results of cord blood methylome, proteome, and metabolome and use a systems approach to allow a better understanding of the full range of 'OMIC' changes in response to micronutrient intervention. Follow-up studies in children will provide an opportunity to investigate the association of these alterations with outcomes of body size and composition, metabolism, and neurocognitive function.

**Supplementary materials.** For supplementary material for this article, please visit <https://doi.org/10.1017/S204017442200068X>

**Data availability statement.** The datasets generated for this study can be found in NCBI SRA: PRJNA756634.

**Acknowledgements.** Ayush Madhok, Indumathi Patta, and Vipul V. Wagh thank CSIR-UGC, Government of India for research fellowships. Satyajeet P. Khare is a beneficiary of the DST SERB SRG grant (SRG/2020/001414). The authors thank Drs Ameya Sathe, Ankitha Shetty for their help in processing cord blood samples, Saurabh Pradhan for help with RNA-seq, Neelam Memane and Rajashree Kamat for laboratory assays, Aboli Bhalerao and Madhura Deshmukh, field staff for their help in the PRIYA study, Mrs. Pallavi Yajnik and Rasika Ladkat for administrative help.

**Author contributions.** Chittaranjan S. Yajnik and Caroline Fall designed the PRIYA trial. Kalyanaraman Kumaran contributed to running the trial. Indumathi Patta assisted in optimisation of cell isolation and RNA preparation. Satyajeet P. Khare and Ayush Madhok performed RNA sequencing and analysis, Satyajeet P. Khare wrote the manuscript. Krishna K. Sukla, Vipul Wagh, and Pooja S. Kunte helped in data analysis and drafting the manuscript. Giriraj R. Chandak and Utpal Tatu contributed to the discussion and interpretations. Deepa Raut and Dattatray Bhat assisted in sample collection. Sanjeev Galande designed the experiments. Chittaranjan S. Yajnik and Sanjeev Galande discussed and interpreted the results, supported the research, and wrote the manuscript. All authors read and approved the manuscript.

**Financial support.** The work was supported by research grant titled "Centre of Excellence in Fetal Programming" from Department of Biotechnology (DBT), Government of India (CEIB-BT/PR12629/MED/97/364/2016) and Indian Council of Medical Research (ICMR) – Medical Research Council (MRC), UK grant (No.58/1/8/ICMR-MRC/2009-NCD-II).

**Conflicts of interest.** The authors have declared no competing interest.

**Ethical Standards.** The authors assert that all procedures contributing to this work comply with the national ethical guidelines for biomedical and health research involving human participants by Indian Council of Medical Research (ICMR) and with the Helsinki Declaration of 1975, as revised in 2008, and have been approved by the King Edward Memorial (KEM) Hospital Research Centre ethics committee.

## References

- Heindel JJ, Vandenberg LN. Developmental origins of health and disease: a paradigm for understanding disease cause and prevention. *Curr Opin Pediatr.* 2015; 27(2), 248–253.
- Lucas A, Fewtrell MS, Cole TJ. Fetal origins of adult disease-the hypothesis revisited. *BMJ.* 1999; 319(7204), 245–249.
- Barker DJ, Winter PD, Osmond C, Margetts B, Simmonds SJ. Weight in infancy and death from ischaemic heart disease. *Lancet.* 1989; 2(8663), 577–580.
- Gluckman PD, Hanson MA, Cooper C, Thornburg KL. Effect of in utero and early-life conditions on adult health and disease. *N Engl J Med.* 2008; 359(1), 61–73.
- Kok DE, Dhonukshe-Rutten RA, Lute C, *et al.* The effects of long-term daily folic acid and vitamin B12 supplementation on genome-wide DNA methylation in elderly subjects. *Clin Epigenet.* 2015; 7(1), 121.
- Switzeny OJ, Mullner E, Wagner KH, Brath H, Aumuller E, Haslberger AG. Vitamin and antioxidant rich diet increases MLH1 promoter DNA methylation in DMT2 subjects. *Clin Epigenet.* 2012; 4(1), 19.
- Zeisel S. Choline, other methyl-donors and epigenetics. *Nutrients.* 2017; 9(5), 445.
- Berry DC, Jin H, Majumdar A, Noy N. Signaling by vitamin A and retinoid-binding protein regulates gene expression to inhibit insulin responses. *Proc Natl Acad Sci U S A.* 2011; 108(11), 4340–4345.
- Pasing Y, Fenton CG, Jorde R, Paulssen RH. Changes in the human transcriptome upon vitamin D supplementation. *J Steroid Biochem Mol Biol.* 2017; 173, 93–99.
- Gernand AD, Schulze KJ, Stewart CP, West KP Jr., Christian P. Micronutrient deficiencies in pregnancy worldwide: health effects and prevention. *Nat Rev Endocrinol.* 2016; 12(5), 274–289.
- Deshmukh U, Katre P, Yajnik CS. Influence of maternal vitamin B12 and folate on growth and insulin resistance in the offspring. *Nestle Nutr Inst Workshop Ser.* 2013; 74, 145–154; discussion 154–146.
- Pandit P, Galande S, Iris F. Maternal malnutrition and anaemia in India: dysregulations leading to the 'thin-fat' phenotype in newborns. *J Nutr Sci.* 2021; 10, e91.
- Rao S, Kanade A, Margetts BM, *et al.* Maternal activity in relation to birth size in rural India. The Pune Maternal Nutrition Study. *Eur J Clin Nutr.* 2003; 57(4), 531–542.
- Yajnik CS, Deshpande SS, Jackson AA, *et al.* Vitamin B12 and folate concentrations during pregnancy and insulin resistance in the offspring: the Pune Maternal Nutrition Study. *Diabetologia.* 2008; 51(1), 29–38.
- Yajnik CS, Chandak GR, Joglekar C, *et al.* Maternal homocysteine in pregnancy and offspring birthweight: epidemiological associations and Mendelian randomization analysis. *Int J Epidemiol.* 2014; 43(5), 1487–1497.
- Wagh RH, Bawdekar RU, Alenaini W, *et al.* Maternal micronutrient status in pregnancy is associated with child's adiposity at 18yrs of age. *J Dev Orig Health Dis.* 2019; 10, S284.
- Kumaran K, Yajnik P, Lubree H, *et al.* The Pune Rural Intervention in Young Adolescents (PRIYA) study: design and methods of a randomised controlled trial. *BMC Nutr.* 2017; 3(1), 41.
- D'Souza N, Behere RV, Patni B, *et al.* Pre-conceptual maternal vitamin B12 supplementation improves offspring neurodevelopment at 2 years of age: PRIYA trial. *Front Pediatr.* 2021; 9, 755977.
- World-Health-Organization. *Composition of a multi-micronutrient supplement to be used in pilot programmes among pregnant women in developing countries: report of a United Nations Children's Fund (UNICEF), World Health Organization (WHO) and United Nations University workshop,* 1999.



20. Frankish A, Diekhans M, Ferreira AM, et al. GENCODE reference annotation for the human and mouse genomes. *Nucleic Acids Res.* 2019; 47(D1), D766–D773.
21. Kim D, Paggi JM, Park C, Bennett C, Salzberg SL. Graph-based genome alignment and genotyping with HISAT2 and HISAT-genotype. *Nat Biotechnol.* 2019; 37(8), 907–915.
22. Liao Y, Smyth GK, Shi W. featureCounts: an efficient general purpose program for assigning sequence reads to genomic features. *Bioinformatics.* 2014; 30(7), 923–930.
23. Love MI, Huber W, Anders S. Moderated estimation of fold change and dispersion for RNA-seq data with DESeq2. *Genome Biol.* 2014; 15(12), 550.
24. Yu G, Wang LG, Han Y, He QY. clusterProfiler: an R package for comparing biological themes among gene clusters. *OMICS.* 2012; 16(5), 284–287.
25. Raudvere U, Kolberg L, Kuzmin I, et al. g:Profiler: a web server for functional enrichment analysis and conversions of gene lists (2019 update). *Nucleic Acids Res.* 2019; 47(W1), W191–W198.
26. Szklarczyk D, Gable AL, Lyon D, et al. STRING v11: protein-protein association networks with increased coverage, supporting functional discovery in genome-wide experimental datasets. *Nucleic Acids Res.* 2019; 47(D1), D607–D613.
27. Bhate V, Deshpande S, Bhat D, et al. Vitamin B12 status of pregnant Indian women and cognitive function in their 9-year-old children. *Food Nutr Bull.* 2008; 29(4), 249–254.
28. Cooper WN, Khulan B, Owens S, et al. DNA methylation profiling at imprinted loci after periconceptional micronutrient supplementation in humans: results of a pilot randomized controlled trial. *FASEB J.* 2012; 26(5), 1782–1790.
29. Fryer AA, Emes RD, Ismail KM, et al. Quantitative, high-resolution epigenetic profiling of CpG loci identifies associations with cord blood plasma homocysteine and birth weight in humans. *Epigenetics.* 2011; 6(1), 86–94.
30. Khulan B, Cooper WN, Skinner BM, et al. Periconceptional maternal micronutrient supplementation is associated with widespread gender related changes in the epigenome: a study of a unique resource in the Gambia. *Hum Mol Genet.* 2012; 21(9), 2086–2101.
31. McKay JA, Groom A, Potter C, et al. Genetic and non-genetic influences during pregnancy on infant global and site specific DNA methylation: role for folate gene variants and vitamin B12. *PLoS One.* 2012; 7(3), e33290.
32. McCullough LE, Miller EE, Mendez MA, Murtha AP, Murphy SK, Hoyo C. Maternal B vitamins: effects on offspring weight and DNA methylation at genomically imprinted domains. *Clin Epigenet.* 2016; 8(1), 8.
33. Caffrey A, Irwin RE, McNulty H, et al. Gene-specific DNA methylation in newborns in response to folic acid supplementation during the second and third trimesters of pregnancy: epigenetic analysis from a randomized controlled trial. *Am J Clin Nutr.* 2018; 107(4), 566–575.
34. Hoyo C, Murtha AP, Schildkraut JM, et al. Methylation variation at IGF2 differentially methylated regions and maternal folic acid use before and during pregnancy. *Epigenetics.* 2011; 6(7), 928–936.
35. Qian YY, Huang XL, Liang H, et al. Effects of maternal folic acid supplementation on gene methylation and being small for gestational age. *J Hum Nutr Diet.* 2016; 29(5), 643–651.
36. Pauwels S, Ghosh M, Duca RC, et al. Dietary and supplemental maternal methyl-group donor intake and cord blood DNA methylation. *Epigenetics.* 2017; 12(1), 1–10.
37. Tserga A, Binder AM, Michels KB. Impact of folic acid intake during pregnancy on genomic imprinting of IGF2/H19 and 1-carbon metabolism. *FASEB J.* 2017; 31(12), 5149–5158.
38. Irwin RE, Thursby SJ, Ondicova M, et al. A randomized controlled trial of folic acid intervention in pregnancy highlights a putative methylation-regulated control element at ZFP57. *Clin Epigenet.* 2019; 11(1), 31.
39. Andraos S, de Seymour JV, O'Sullivan JM, Kussmann M. The impact of nutritional interventions in pregnant women on DNA methylation patterns of the offspring: a systematic review. *Mol Nutr Food Res.* 2018; 62(24), e1800034.
40. James P, Sajjadi S, Tomar AS, et al. Candidate genes linking maternal nutrient exposure to offspring health via DNA methylation: a review of existing evidence in humans with specific focus on one-carbon metabolism. *Int J Epidemiol.* 2018; 47(6), 1910–1937.
41. Bhat DS, Thuse NV, Lubree HG, et al. Increases in plasma holotranscobalamin can be used to assess vitamin B-12 absorption in individuals with low plasma vitamin B-12. *J Nutr.* 2009; 139(11), 2119–2123.
42. Deshmukh US, Joglekar CV, Lubree HG, et al. Effect of physiological doses of oral vitamin B12 on plasma homocysteine: a randomized, placebo-controlled, double-blind trial in India. *Eur J Clin Nutr.* 2010; 64(5), 495–502.
43. Lager S, Powell TL. Regulation of nutrient transport across the placenta. *J Pregnancy.* 2012; 2012, 179827–14.
44. Whitfield ML, George LK, Grant GD, Perou CM. Common markers of proliferation. *Nat Rev Cancer.* 2006; 6(2), 99–106.
45. Yadav DK, Shrestha S, Lillycrop KA, et al. Vitamin B(12) supplementation influences methylation of genes associated with Type 2 diabetes and its intermediate traits. *Epigenomics.* 2018; 10(1), 71–90.
46. Blomhoff HK. Vitamin A regulates proliferation and apoptosis of human T- and B-cells. *Biochem Soc Trans.* 2004; 32(Pt 6), 982–984.
47. MacDonald RS. The role of zinc in growth and cell proliferation. *J Nutr.* 2000; 130(5S Suppl), 1500S–1508S.
48. Umar M, Sastry KS, Chouchane AI. Role of vitamin D beyond the skeletal function: a review of the molecular and clinical studies. *Int J Mol Sci.* 2018; 19(6), 1618.
49. Boon R, Silveira GG, Mostoslavsky R. Nuclear metabolism and the regulation of the epigenome. *Nat Metab.* 2020; 2(11), 1190–1203.
50. Antony A. Megaloblastic anemias. In *Hematology: Basic Principles and Practice* (eds. Hoffma R, Benz EJ, Silberstein LE, et al.), 2017. Elsevier, Philadelphia, PA.
51. Battaglia-Hsu SF, Akchiche N, Noel N, et al. Vitamin B12 deficiency reduces proliferation and promotes differentiation of neuroblastoma cells and up-regulates PP2A, proNGF, and TACE. *Proc Natl Acad Sci U S A.* 2009; 106(51), 21930–21935.
52. Rzepka Z, Rok J, Respondek M, et al. Cobalamin deficiency: effect on homeostasis of cultured human astrocytes. *Cells.* 2019; 8(12), 1505.
53. Lyon P, Strippoli V, Fang B, Cimmino L. B vitamins and one-carbon metabolism: implications in human health and disease. *Nutrients.* 2020; 12(9), 2867.



## OPEN ACCESS

## EDITED BY

Subashika Govindan,  
Wellcome Trust DBT India Alliance, India

## REVIEWED BY

Claire Cheetham,  
University of Pittsburgh, United States  
René Oliver Goral,  
National Institute of Environmental Health  
Sciences (NIH), United States

## \*CORRESPONDENCE

Nixon M. Abraham  
✉ nabraham@iiserpune.ac.in  
Sanjeev Galande  
✉ sanjeev@iiserpune.ac.in

<sup>†</sup>These authors have contributed equally to this work

RECEIVED 06 March 2023

ACCEPTED 15 May 2023

PUBLISHED 19 June 2023

## CITATION

Mahajan S, Sen D, Sunil A, Srikanth P, Marathe SD, Shaw K, Sahare M, Galande S and Abraham NM (2023) Knockout of angiotensin converting enzyme-2 receptor leads to morphological aberrations in rodent olfactory centers and dysfunctions associated with sense of smell.  
*Front. Neurosci.* 17:1180868.  
doi: 10.3389/fnins.2023.1180868

## COPYRIGHT

© 2023 Mahajan, Sen, Sunil, Srikanth, Marathe, Shaw, Sahare, Galande and Abraham. This is an open-access article distributed under the terms of the [Creative Commons Attribution License \(CC BY\)](https://creativecommons.org/licenses/by/4.0/). The use, distribution or reproduction in other forums is permitted, provided the original author(s) and the copyright owner(s) are credited and that the original publication in this journal is cited, in accordance with accepted academic practice. No use, distribution or reproduction is permitted which does not comply with these terms.

# Knockout of angiotensin converting enzyme-2 receptor leads to morphological aberrations in rodent olfactory centers and dysfunctions associated with sense of smell

Sarang Mahajan<sup>1,2†</sup>, Deepshikha Sen<sup>1,2†</sup>, Anantu Sunil<sup>1,3†</sup>, Priyadharshini Srikanth<sup>1,2</sup>, Shruti D. Marathe<sup>1,2</sup>, Karishma Shaw<sup>1,2</sup>, Mahesh Sahare<sup>2</sup>, Sanjeev Galande<sup>2,4,5\*</sup> and Nixon M. Abraham<sup>1,2\*</sup>

<sup>1</sup>Laboratory of Neural Circuits and Behaviour (LNCB), Department of Biology, Indian Institute of Science Education and Research (IISER), Pune, Maharashtra, India, <sup>2</sup>Department of Biology, Indian Institute of Science Education and Research (IISER), Pune, Maharashtra, India, <sup>3</sup>Indian Institute of Science Education and Research (IISER), Kolkata, West Bengal, India, <sup>4</sup>Laboratory of Chromatin Biology and Epigenetics, Department of Biology, Indian Institute of Science Education and Research (IISER), Pune, Maharashtra, India, <sup>5</sup>Center of Excellence in Epigenetics, Department of Life Sciences, Shiv Nadar University, Delhi-NCR, India

Neuronal morphological characterization and behavioral phenotyping in mouse models help dissecting neural mechanisms of brain disorders. Olfactory dysfunctions and other cognitive problems were widely reported in asymptomatic carriers and symptomatic patients infected with Severe Acute Respiratory Syndrome Coronavirus-2 (SARS-CoV-2). This led us to generate the knockout mouse model for Angiotensin Converting Enzyme-2 (ACE2) receptor, one of the molecular factors mediating SARS-CoV-2 entry to the central nervous system, using CRISPR-Cas9 based genome editing tools. ACE2 receptors and Transmembrane Serine Protease-2 (TMPRSS2) are widely expressed in the supporting (sustentacular) cells of human and rodent olfactory epithelium, however, not in the olfactory sensory neurons (OSNs). Hence, acute inflammation induced changes due to viral infection in the olfactory epithelium may explain transient changes in olfactory detectabilities. As ACE2 receptors are expressed in different olfactory centers and higher brain areas, we studied the morphological changes in the olfactory epithelium (OE) and olfactory bulb (OB) of ACE2 KO mice in comparison with wild type animals. Our results showed reduced thickness of OSN layer in the OE, and a decrease in cross-sectional area of glomeruli in the OB. Aberrations in the olfactory circuits were revealed by lowered immunoreactivity toward microtubule associated protein 2 (MAP2) in the glomerular layer of ACE2 KO mice. Further, to understand if these morphological alterations lead to compromised sensory and cognitive abilities, we performed an array of behavioral assays probing their olfactory subsystems' performances. ACE2 KO mice exhibited slower learning of odor discriminations at the threshold levels and novel odor identification impairments. Further, ACE2 KO mice failed to memorize the pheromonal locations while trained on a multimodal task implying the aberrations of neural circuits involved in higher cognitive functions. Our results thus provide the morphological basis for the sensory and cognitive disabilities caused by the deletion of ACE2 receptors and offer a potential experimental approach to study the neural circuit mechanisms of cognitive impairments observed in long COVID.



## KEYWORDS

ACE2 receptor, gene knockout, CRISPR-Cas9, olfactory system, sensory and cognitive deficits

## 1. Introduction

Angiotensin converting enzyme (ACE) 2 plays a critical role in maintaining physiological homeostasis (Donoghue et al., 2000; Hamming et al., 2004). It is widely expressed in different body systems and was identified as one of the molecular factors mediating Coronavirus disease 2019 (COVID-19) infection (Brann et al., 2020; Fodouliau et al., 2020; Hoffmann et al., 2020). Most of the mortality caused by COVID-19 infection have been reported to be due to severe respiratory problems. This was caused by malfunctioning of cardiovascular and respiratory systems (Crackower et al., 2002; Hoffmann et al., 2020). The defects associated with lung function can be a predictor for neurological impairments as well (Mahmmedi et al., 2021). Since the beginning of pandemic, autopsy studies reported the presence of viral particles in multiple organ systems including the nervous system (Puelles et al., 2020). Brain imaging data further confirmed the structural abnormalities caused by the viral infection (Douaud et al., 2022). Moreover, long-lasting brain dysfunctions have become a serious challenge in post-COVID-19 conditions (Pardasani and Abraham, 2022; Bhowmik et al., 2023). Therefore, probing the mechanisms underlying these deficits using animal models is a pressing need of global health.

The binding of viral particles on ACE2 receptors leads to the creation of a fusion pore that allows viral entry into the host cells. This is assisted by the priming of spike protein by host cell transmembrane protease, serine 2 (TMPRSS2) (Shang et al., 2020; Jackson et al., 2022). Although the routes of viral entry to the central nervous system (CNS) and the neurotropism of Severe Acute Respiratory Syndrome Coronavirus 2 (SARS-CoV-2) remain as debated topics, various cellular factors mediating virus entry are expressed in neuronal and non-neuronal cells in the brain (Pardasani and Abraham, 2022). ACE2 receptors are expressed in the non-neuronal supporting (sustentacular) cells of olfactory epithelium. This explains the prevalent olfactory deficits caused by different strains of SARS-CoV-2 (Bhattacharjee et al., 2020; Whitcroft and Hummel, 2020; Iravani et al., 2022), supported by the observations on presence of viral RNA and protein in the nasopharynx (Meinhardt et al., 2021). However, some studies did not find the presence of viral particles in the olfactory sensory neurons (OSNs) and olfactory bulb (OB), leading to the debate on the neurotropism of SARS-CoV-2 (Khan et al., 2021). Another receptor type that facilitates virus entry, Neuropilin-1 (NRP1) is expressed in the neurons, olfactory epithelial cells, and endothelial cells etc. (Cantuti-Castelvetri et al., 2020; Kyrou et al., 2021). Despite the above-mentioned evidence on molecular factors, studies dissecting the neural basis of olfactory and cognitive deficits using animal models are scarce.

Single cell sequencing studies of mouse olfactory epithelium revealed the expression of ACE2 and TMPRSS2 in the sustentacular cells, however not in the OSNs (Brann et al., 2020; Fodouliau et al., 2020; Hoffmann et al., 2020). Transnasal infusion of viral particles in Golden Syrian Hamsters provided the evidence for neuronal invasion.

Both neuronal and non-neuronal cell deaths were observed during the post-infection period (De Melo et al., 2021). As genetic approaches mimicking viral infection can provide stable readouts, we decided to generate ACE2 receptor knockout using CRISPR-Cas9 genome editing tools. The CRISPR-Cas9 technique has been successfully used in mouse and other mammalian species to generate genetically modified animals (Shao et al., 2014; Kang et al., 2019). The deletion of ACE2 gene was ensured by targeting the crucial translational start site of the exon 2 and verified by sequencing. On generating ACE2 KO mice, we carried out the morphological studies and the behavioral phenotyping focusing on the functioning of olfactory system. As olfactory problems of varying severity including hyposmia, anosmia and parosmia are observed during and post-COVID conditions, we used well-established and sensitive behavioral assays (Abraham et al., 2004, 2010, 2014; Bhattacharjee et al., 2019; Pardasani et al., 2021). The reduced thickness of OSN layer and the lowered MAP2 immunoreactivity in the glomerular region explained various olfactory problems including the detection, and discrimination deficits at the threshold levels and the lowered novel odor identification abilities. Further, ACE2 KO mice showed compromised pheromone location learning, which involved more than one sensory modality. Hence, our experimental approach would facilitate probing the neural mechanisms of long-COVID complications.

## 2. Materials and methods

### 2.1. Maintenance of animals

A total of 119 C57BL/6J and ACE2 KO male and female adult mice were used for all of the experiments in this study. The mice were between 6 to 8 weeks old at the beginning of the experiment. 12-h light/dark cycle was maintained and mice were grouped in individually ventilated cages in a temperature- and humidity-controlled animal facility. Mice had unlimited access to food, but were subjected to a water restriction schedule meant to keep them at >80% of their baseline body weight during Go/No-Go behavioral training. The schedule of water restrictions was never longer than 12h. All animal care and procedures were in accordance with the Institutional Animal Ethics Committee (IAEC) at IISER Pune and the Committee for the Purpose of Control and Supervision of Experiments on Animals (CPCSEA), Government of India.

### 2.2. Generation of ACE2 KO mouse model

Using CRISPR-Cas9 gene targeting technology, we generated a knockout mouse model for ACE2. The knockout was created by specifically targeting the translation start site (TSS), which lies in the exon 2 of the ACE2 gene (Figure 1A). Guide RNAs for the 5' and 3' ends of the targeted region were chosen to generate the knockout

(ATCAGCCTTTGAACTTGGGT; ATCAAAGTTCACCTTGCTTCT). SgRNAs were designed using the CRISPOR online tool<sup>1</sup> and synthesized by Sigma Aldrich.

## 2.3. Microinjection of one-cell embryos

C57BL/6J mice at 3–4 weeks of age were superovulated by intraperitoneal injection of 5 IU pregnant mare serum gonadotropin (PMSG), followed by injection of 5 IU human chorionic gonadotropin (Sigma Aldrich) after 48 h. Mouse zygotes were obtained by mating C57BL/6J stud males with superovulated C57BL/6J females. One-cell stage fertilized mouse embryos were injected with CRISPR components mixed in microinjection buffer. The final concentrations of Cas9 protein and sgRNA were 50 ng/μL and 25 ng/μL, respectively. The fertilized one cell embryos were isolated from superovulated female mice. Microinjection of the mixture was performed into pronuclei of fertilized eggs using FemtoJet 4i microinjector with manipulator (Eppendorf) attached to IX83 microscope (Olympus). The injected embryos were transferred into the oviduct of pseudo-pregnant females to allow further development. Microinjections and mouse transgenesis experiments were performed as described previously (Harms et al., 2014).

The resulting pups were genotyped for founder screening. The primers used for PCR were (ACE2-F1: 5'- ACCCTCCTCCTCCAGTG TAT -3' and ACE2-R1: 5'- AGGCAGTCACTCATCCTCAC -3'). PCR was conducted using the following conditions: Initial denaturation at 95°C for 4 min, 36 cycles with denaturation at 94°C (30 s), annealing at 60°C (30 s), and extension at 68°C (1 min). Final extension was performed at 68°C for 5 min. The deletion of the ACE2 gene's target site in mice was identified and confirmed by using polymerase chain reaction (PCR) and gene sequencing. The sequence confirmed founders were backcrossed to wild-type C57BL/6J mice for two consecutive generations and the founder line was established. Animals with confirmed ACE2 receptor gene knockout were used for breeding.

## 2.4. Western blotting

For Western Blotting (WB), 6–10 weeks old wild type and ACE2 KO animals were used. Mouse brains were dissected and stored at -80°C. Whole brain lysates were prepared in RIPA buffer supplemented with cOmplete protease inhibitor (Roche Cat # 04693116001). Protein estimation was performed using Pierce BCA protein assay kit (ThermoFisher Cat # 23225). Fifteen μg of the sample was loaded in each well of 12% acrylamide gel and SDS-polyacrylamide gel electrophoresis (PAGE) was performed. The proteins were then transferred to Immobilon-P PVDF membranes (Millipore Cat # IPVH00010). Blocking was performed with 5% milk/Tris-buffered saline-Tween 20 for 1 h at room temperature. The membranes were probed with primary anti-ACE2 antibody (Abcam Cat # 15348) and anti-GAPDH (Sigma Cat # G9545) at 1:1000 and 1:5000 dilutions, respectively at 4°C for 16 h. The secondary antibody used was peroxidase-conjugated AffiniPure Goat anti-rabbit IgG

(Jackson ImmunoResearch Cat # 111-035-003) at 1:5000 dilution for 1 h at room temperature. Bound antibody was detected using Clarity ECL Western Blotting Substrate (BioRad Cat # 1705061) with the image digitally captured using an ImageQuant LAS 4000 imager.

## 2.5. Hematoxylin and eosin staining of olfactory epithelium

The mice were initially perfused with 1 × Phosphate Buffer Saline (PBS) followed by 4% paraformaldehyde. The animal was decapitated, and the nasal cavity was dissected. After that, tissue was kept for a week in a 10% Ethylenediamine tetraacetic acid (EDTA) solution to decalcify the bones that surround the nasal cavity. After the removal of tissue from the EDTA solution, the nasal cavity was extracted by delicately removing the surrounding bones. Following the dissection of the nasal cavity, it was embedded in the paraffin wax. Briefly, the nasal cavity was kept in 60% isopropanol (90 min × 3 times), 80% isopropanol (45 min × 2 times), 90% isopropanol (30 min × 1 time followed by 15 min × 1 time), and then in xylene (15 min × 3 times). The dehydrated nasal cavity was then placed over previously melted paraffin wax and incubated overnight at 62°C in an oven. Following that tissue was embedded in a wax block and was incubated at -20°C overnight. Using microtome (RM2235, Leica Biosystems), 5–8 μm sections were obtained and were transferred to the poly-L-lysine coated slides. The slides were then incubated in a hybridization oven overnight at 62°C. Then, the slides were kept in xylene (5 min × 2 times) followed by varying concentrations of ethanol: 100, 90, 70, and 50% for 3 min each. The slides were then kept in distilled water for 3 min. The slides were removed from the water and left to air dry. A napkin was used to wipe away any excess water surrounding the tissue. Slides were positioned on the rails of the humidifying chamber, and a drop of hematoxylin was applied to the tissue and slides were left undisturbed for 15 min. The excess hematoxylin stain was removed with distilled water, and the slides were rinsed under running water for 15 min. The slides were then submerged for 10 s in 80% ethanol containing 1% Hydrochloric acid (HCl). To each tissue section, a drop of eosin was added. After 30 s of eosin application, slides were transferred to 70% ethanol for 1 min, 90% ethanol for 1 min, and 100% ethanol for 1 min. The slides were taken out of the ethanol and let to air dry. Following that slides were kept in xylene (15 min × 2 times). The slides were taken out, and before the slides dried fully, excess xylene was removed from the corners of the slides using a napkin and a drop of DPX medium was applied to the sections. The slides were mounted with a cover slip and edges of the cover slip were sealed. A brightfield microscope (BX43, Olympus) was next used to examine the sections and capture the images. We selected similar regions in the medio-lateral and antero-posterior axes on the nasal turbinates for both WT and KO mice. While calculating the cumulative distributions, 3–4 regions of interest (ROIs) from 18 to 24 sections per animal were selected to cover the nasal epithelium (Figure 2D). In addition, we have measured the epithelial thickness in different areas near to the septum (henceforth named as septal areas, dorsomedial and middle meatus areas) and other turbinate regions toward the lateral side (ethmoturbinate areas) in each section, with similar numbers from both locations (Supplementary Figure S1). The thickness of OE was measured across OSN layer at different locations (as marked in Figures 2B1,B2).

<sup>1</sup> <http://crispor.tefor.net/>

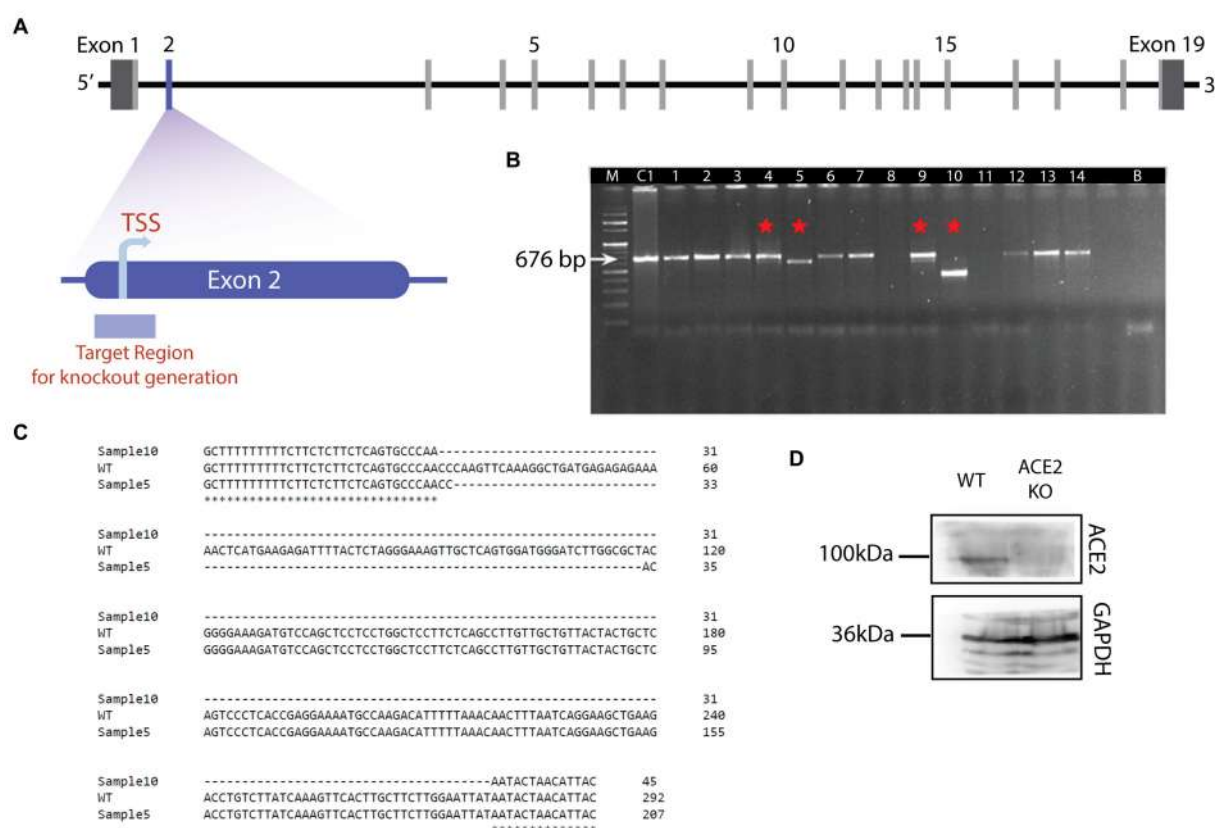


FIGURE 1

Generation of ACE2 knockout mouse model. **(A)** Schematic of the genetic structure of the ACE2 gene. ACE2 gene harbors 19 exons with the translation start site (TSS) in the exon 2. TSS is the target region to create the knockout using CRISPR-Cas9 mediated genome editing. **(B)** Agarose gel electrophoresis image of DNA samples isolated from the potential ACE2 KO animals. Sample C is the control (C57BL/6J) genomic DNA (676bp), Sample B is used as a negative control without any genomic DNA, and samples 1 to 14 are DNAs with genome editing. Samples 4, 5, 9, and 10 revealed the deletions and are depicted by red asterisk on the gel. Sample 10 showed the maximum deletion, hence selected for further breeding. **(C)** Sequence alignment showing deletions in samples 5 and 10. For the sample 5, 84bp deletion was observed, whereas for sample 10, a 246bp deletion occurred in the target region. These results confirmed the deletion of the ACE2 receptor gene in sample 10. **(D)** Western blot showing the expression of ACE2 protein in the brain of ACE2 KO and WT animals. The band corresponding to ACE2 protein was observed for WT animals, whereas in ACE2 KO animals, ACE2 expression was undetectable. Band corresponding to GAPDH protein is observed in brain lysates from both animals.

## 2.6. Immunohistochemistry using MAP2

ACE2 KO and WT animals were perfused, and their olfactory bulbs (OB) were dissected. The dissected brain was kept in 4% paraformaldehyde for 24 h before keeping it in 30% sucrose for 1 day for cryoprotection. For Microtubule associated protein 2 (MAP2) staining, 50  $\mu$ m thick sections were obtained using cryotome (CM1950, Leica Biosystems) and one section was selected for every five sections. Sections were washed three times in tris-buffered saline (1  $\times$  TBS) for 15 min on a rocker at 15 rpm. The permeabilization and blocking were done using TBST (0.2% Triton X-100 in 1  $\times$  TBS) with 5% bovine serum albumin (BSA) and 7.5% normal goat serum (NGS) for 1 h at room temperature. The sections were then incubated overnight at 4°C with primary antibody diluted in the respective blocking buffers. Chicken anti-MAP2 (Abcam, ab92434, 1:3000) was used as the primary antibody. Sections were then washed with 1  $\times$  TBS (10 min  $\times$  3 times) and incubated for 1 h at room temperature with secondary antibody diluted in TBST. Alexa Fluor 647-conjugated donkey anti-chicken IgG (Jackson ImmunoResearch, 703-605-155, 1:500) was used as the secondary antibody. The sections were

then given 1  $\times$  TBS (10 min  $\times$  3 times) washes and were incubated with DAPI (Sigma, 1:500) in 1  $\times$  TBS for 10 min. Following that, sections were washed once with 1  $\times$  TBS (10 min) and then mounted onto slides with glass coverslips using a mounting medium. The mounted sections were imaged using a confocal microscope (SP8, Leica Biosystems). All image acquisition parameters, such as the objective (40X oil immersion), zoom (1.0), pinhole diameter (1 AU), pixel format (1024  $\times$  1024), laser intensity (~5%), and scanned thickness of ~20  $\mu$ m (1  $\mu$ m step size), were kept constant during the imaging.

The area of the glomeruli and the MAP2 immunoreactivity were quantified from maximum intensity projection (MIP) images containing two channels: DAPI and MAP2 (Figure 2E, Blue and Green color, respectively). In the MIP images, each glomerulus representing an ROI was selected using the freehand selection tool in ImageJ/Fiji. The area and mean gray value (MAP2 channel) were measured for each glomerulus. To rule out any sampling bias that may result from the size distribution of glomeruli in the whole OB, we took every fifth coronal section of the OB (50  $\mu$ m sections, 12–14 sections of both OBs per mouse) covering the entire anterior–posterior axis.

Similar numbers of ROIs were selected in mediolateral and dorsoventral axes in both WT and ACE2 KO mice.

## 2.7. Go/no-go odor discrimination

### 2.7.1. Odors

For Go/No-Go discrimination task, following odors were used: Methyl Benzoate (MB), Limonene (+) (Li), Amyl acetate (AA), and Ethyl butyrate (EB). The odors were diluted in mineral oil (MO) and different dilution of the odors were used ( $10^{-4}$  to  $10^{-10}$  percent volume in MO). All odors had a purity level of above 99% and were purchased from Sigma-Aldrich, and the mineral oil was obtained from Oswal Pharmaceuticals in Pune, Maharashtra, India.

### 2.7.2. Odor pairs

Different sets of animals were trained to differentiate the following: Li vs. MO ( $10^{-10}$ ,  $10^{-9}$ , and  $10^{-8}$ % v/v), MB vs. MO ( $10^{-10}$ ,  $10^{-8}$ , and  $10^{-6}$ % v/v), and complex binary mixture of AA vs. EB [AA(60%) + EB(40%) vs. EB(60%) + AA(40%)] ( $10^{-8}$ ,  $10^{-6}$ , and  $10^{-4}$ % v/v).

### 2.7.3. Apparatus

For olfactory-based discrimination experiments, eight-channel olfactometer with custom modifications was used (Knosys). The apparatus consisted of an operant chamber where the animal was kept during the behavioral test. The operant chamber has a combined odor sampling and reward port on one side that is guarded by an IR beam. This allows for a tight association between odor presentation in a trial and the reward. A trial is initiated when the animal breaks the IR beam by poking its head into the sampling port. The odor valve connected to a flowmeter opens as the trial initiates and it controls the onset and flow of odor stream (airflow rate of 2 Liters per min). After 500 ms of odor valve opening, a final valve (diversion valve) that lies near to the sampling port, opens and the stimulus is delivered to the animal. The precise onset of the stimulation was ensured by a system of these solenoid valves that are controlled by custom written program in IGOR. The S+ (rewarded) or the S- (non-rewarded) odors were presented through a set of different valves.

### 2.7.4. Task-habituation phase

The animals were subjected to task habituation training three to 4 days after the beginning of the water deprivation schedule. Standard operant conditioning approaches were used to train the animals. The task habituation phase was performed for the animals to get acclimatized to the operant chamber, location of reward and sampling port, lick tube, sounds of the valves, and procedural aspects of the instrument. The task habituation consisted of nine phases (Phase 0–8). In the Phase 0, animal received water reward (3–5  $\mu$ L) simply by breaking the IR beam. This enabled the animals to locate the reward port and the water delivery tube. In the following phase, the animals were given water only when they made at least one lick. For the subsequent stages of this task-habituation training, the complexity level of the task increased gradually, and animals had to lick on the tube in order to receive the water reward. In the late stages of this phase, odor valve was introduced and animal received the odor stimulus for 2 s, wherein animal has to respond and lick to receive the

reward. All animals finished the task habituation phase in three to four sessions of 30 min.

### 2.7.5. Discrimination training phase

The odor-based discrimination tasks were performed using a Go/No-Go behavioral paradigm (Abraham et al., 2004). The mouse initiated a trial by breaking the IR beam that was guarding the sampling port. This enabled the opening of one of the solenoid valves, followed by the opening of a three-way diversion valve after 500 milliseconds. After diversion valve is opened the stimulus is presented to the animal for a 2 s duration. The use of a diversion valve reduced the period between the onset of the stimulus and the first contact with the animal. To obtain a reward, the animal has to meet the required reward criteria based on the reward contingency of the stimulus [Rewarded (S+)/ Non-Rewarded (S-)].

The time that was provided for animals to respond overlapped with the stimulus duration. The response time was virtually divided into four equal bins, i.e., for a response/stimulus duration of 2 s, divided into four 500 ms bins. Animals required to register a lick in at least three out of these four bins for a S+ trial to be considered correct. For a successful S+ trial, a water reward of 3–4  $\mu$ L was given to the animal after the stimulus ended [Reward Criteria: Animal needs to register a lick in at least three out of the four bins]. For an S- trial to be correct, animal was only allowed to lick for at most two bins. There was no punishment or reward for an incorrect or correct S- trial, respectively. Before the next trial could be initiated, a 5-s inter-trial interval (ITI) was kept. There were no rules requiring the mouse to smell the odor for a certain amount of time before making a choice and to prohibit licking prior to the odor. The mice received stimuli in blocks of 20 trials. Ten S+ trials and ten S- trials were present in each of these blocks. Within a block, the S+ and S- trials were pseudorandomized in order to prevent the delivery of more than two consecutive stimuli with the same reward condition. The preference for a particular stimulus was prevented by balancing the S+ and S- stimuli for a group of animals (for instance, in a group of 8 animals, 4 mice receive one stimulus as S+ while the other 4 animals receive another stimulus as S+). The animals were adequately motivated to finish 200–300 trials in a day, spaced out over 1–2 (30–40 min) sessions. Animal's motivation was measured using different instrumental readouts, including licking probability and inter-trial interval. The training session was terminated after the animal stopped licking for the rewarded trials. The data was collected using a custom-written software in IGOR-PRO that was compatible with the MCC-CIO-DIO 48 data acquisition card.

### 2.7.6. Behavioral readouts

#### 2.7.6.1. Learning curve

The learning curve measures the performance as the percentage of correct responses during the training. Each point on the learning curve indicates the average accuracy of 100 trials [50S+ and 50S-] across all animals.

#### 2.7.6.2. D-prime ( $d'$ )

Hit (correct S+) and false alarm (incorrect S-) probabilities were computed for  $d'$  over an average of 100 trials. The probabilities were used to calculate the z-score.  $d'$  was calculated as  $z(\text{hit}) - z(\text{false alarm})$  per 100 trials.



### 2.7.6.3. Discrimination time

The licking behavior of each mouse was monitored to assess the discrimination time. Animals' licking behavior was recorded with high temporal resolution and analyzed in time bins of 20 ms. The licking behavior changed as a result of learning and was considerably different between the early and late stages of learning. During the early phase of learning, when the animals were not able to discriminate the S+ and S- stimuli, they licked for both the stimuli. As a result, during the initial training phase, the animal's lick responses to S+ and S- stimuli were comparable. But as soon as they were able to differentiate between two stimuli, they began to selectively lick for S+ trials and avoid licking for S- trials, which caused a divergence in the lick responses between two stimuli. The statistical comparison of the lick responses between the S+ (150 trials) and S- (150 trials) trials was performed using one-tailed t-test. The t-test was performed for each time bin of the lick pattern between S+ and S- trials. This comparison yields a value of p curve as a function of time. In the value of p curve, the last time point where the value of p is  $<0.05$  is taken as the discrimination time. The discrimination time was measured task wise, i.e., for 300 trials.

### 2.7.6.4. Area under the curve (AUC)

The area under the curve (AUC) was also used to calculate the discrimination index of the animals. For AUC calculations, the lick probabilities for S+ and S- trials were used. The discrimination index was calculated as:  $AUC = (AUC_{S+} - AUC_{S-}) / AUC_{S+}$ .

## 2.8. Novel odor discrimination

To further compare the novel odor discrimination abilities of ACE2 KO mice with WT mice, a previously published olfactory habituation/dishabituation paradigm with slight modifications was adopted (Tillerson et al., 2006; Lehmkuhl et al., 2014). Before the experiment began, animals were kept in the experimental cage for 5 min for cage habituation. 50  $\mu$ L of distilled water or odor (diluted to 1% in mineral oil) was applied on a piece of Whatman filter paper and kept inside separate, identical boxes at the two ends of a cage. For the first trial, the box containing water was placed on one side of the cage, and the box containing the odor (cineole or eugenol) was placed on the opposite side. One trial continued for 3 min during which the behavior of animals was recorded. The boxes were removed from the cage after the trial finished. Inter-trial interval of 15 min were provided between the trials. In order to prevent any location-based bias of the animal, the cage was rotated around 180° between each trial. Only one odor was used for the first five trials to ensure the odor habituation, following which, on the 6<sup>th</sup> trial, this odor was replaced with a novel odor, e.g., if eugenol was used in the first five trials (habituated odor), it was replaced with cineole (novel odor) in the 6<sup>th</sup> trial. For each trial the behavior of animal was videotaped and the trial videos were analyzed using EthoVision software. The amount of time the animal spent sampling a particular box was determined by how long its nose tip was inside a region around 2 cm from the perimeter of the box. These areas were chosen as the zones in the software, while the entire cage served as the arena. The cage's length and width were used to calibrate the arena, and a sample rate of 30.00 samples per second was used. Dynamic subtraction was used to identify the mice's nose, center, and base of tail at a dark contrast of 50–60.

## 2.9. Pheromone detection

An open field pheromone detection experiment was used to examine the pheromone detecting capacities of ACE2 KO and wild type females. Before the experiment began, all females had attained sexual maturity. The behavioral apparatus used to assess pheromonal detectabilities comprised of a chamber with dimensions of 60 cm x 45 cm. Since non-volatile odorants are found in male-soiled bedding, and volatile odorants are found in urine, the test was conducted by placing a petri dish filled with male soiled bedding and urine (~100  $\mu$ L) at the center of the arena. Females were kept in the chamber for 10 min and were allowed to freely roam and explore the arena. A camera was used to record the animals' movements, and EthoVision software was used to track them. The amount of time the females spent in the vicinity of the petri dish was used to quantify the sampling behavior.

## 2.10. Multimodal pheromonal learning

### 2.10.1. Apparatus

Pheromone preference and odor association abilities in mice were tested using the multimodal pheromonal learning paradigm established in our lab (Pardasani et al., 2021). For this experiment, the same groups of females that were used for the pheromone detection experiment were used. The apparatus comprised of an arena with dimensions of 60 cm x 30 cm x 15 cm (length x width x height). The entire arena was divided into three spaced zones having equal areas with the help of two sliding partitions. Opening both the partitions allowed the females to explore the entire arena, whereas closing them allowed us to restrict the females in specific areas. At the opposite extremities of the arena, two 10 cm x 10 cm x 15 cm compartments with removable plates were positioned. In each chamber, a 55 mm petri dish held 100  $\mu$ L of either water (the neutral stimulus in chamber 2) or urine (the attractive pheromonal stimulus in chamber 1) was kept. These chambers were guarded by the lids having orifices with different diameters (5 mm and 10 mm). Due to this, the animal was restricted to sample the volatiles coming from the chamber's front side through the holes and they were able to associate the diameters with the volatile cues. To mitigate any bias toward the diameters of the holes, animals were counterbalanced for the association between the volatile cues and the different orifice sizes.

### 2.10.2. Paradigm

The experimental design included a 4-day initial testing phase, a 15-day training phase, and memory tests on the 15th day after the training. The purpose of the initial testing phase was to determine whether female mice have an intrinsic preference for the zones (zone 1 containing the volatile and non-volatile pheromones from male mice & zone 2 containing neutral stimuli, water). During the early testing and training phases, the equipment was rotated by 180° every day to eliminate any directional bias toward a specific zone. Following the initial testing phase, 15 days of training was performed. During the training phase, each day, the animal was only allowed in one of the zones for 15 min (alternating between the two zones after every 5 min, 3 times). Fifteen days after the end of training phase, memory test was performed. To test the memory, all volatile and



non-volatile pheromonal stimuli (urine and soiled bedding with non-volatile pheromonal traces) and neutral water stimuli were removed from the chambers of the apparatus while leaving the plates with specific diameter orifices undisturbed. Using the EthoVision program, the amount of time spent in each zone, particularly in front of chambers 1 and 2, was quantified. Animal tracks were visualized and time spent was calculated using EthoVision's nose point feature, which is used to track animals. The number of active attempts on the plates guarding chambers 1 and 2 was manually scored by counting each nose poke through the plate as one attempt. Memory index was calculated for both the time spent and number of active attempts as:  $\text{Memory Index} = (\text{Time spent or No. of active attempts in pheromone zone} - \text{Time spent or No. of active attempts in neutral stimulus zone}) / \text{Time spent or No. of active attempts in neutral stimulus zone}$ .

## 2.11. Behavioral tests for stress, anxiety, and motor control

Different tests were conducted to study the exploration, anxiety-like, and depression related behaviors and motor control of the animals. These tests were conducted in the following order:

### 2.11.1. Open field test

The set-up consisted of a pseudo home cage where mice belonging to the same cage were housed for about 15 min. The dimension of the cage was 42 cm x 26 cm x 18 cm and the top of the cage was covered with a grill. In order to prevent any initial hyperactivity, the animals were acclimated in this cage. During the test, a single mouse was permitted to pass from the cage into the main arena (60 cm x 45 cm) through a little opening for 10 min. A camera mounted on a tripod stand captured the exploratory behavior of the animal. Using EthoVision tracking software, the total distance traveled, time spent in the center of the arena, latency to the center, and total time spent in the four corners were calculated.

### 2.11.2. Elevated plus maze test

For EPM test, an elevated plus maze which was raised 50 cm above the ground was used. The apparatus constituted closed and open arms. The arms of the maze were 5 cm wide and 55 cm long. The closed arms consisted of walls that were 15 cm high. The middle zone at the junction of the four arms had a dimension of 5 cm x 5 cm. To initiate a trial, the animal was placed on this junction facing the open arm. The trials lasted for 5 min and animals were free to explore the EPM during this time. For quantitative analysis, the time spent in open vs. closed arms and the number of entries into the open and closed arms were calculated.

### 2.11.3. Tail suspension test

For TST, mouse was suspended by its tail using a 15 cm piece of tape attached to a horizontal rod at a height of 40 cm from the ground. Each trial lasted for 6 min, following which the animals were removed from the apparatus. For analysis, time spent mobile, where the animal tries to escape, and the time spent immobile were quantified manually with a resolution of 1 s.

### 2.11.4. Forced swim test

FST was performed using an acrylic cylinder of 15 cm diameter and 30 cm height that was filled with water (12 cm height). The mouse was placed in the water for 6 min. To prevent hypothermia after the experiment was finished, the mouse was placed in a cage covered with dry tissue which was kept on a heating pad for 15 min. The animal was then transferred to its native cage. Behavior of the animal was classified between the time spent mobile and immobile. The mobility and immobility were scored manually with a resolution of 1 s. Across ACE2 KO and wild type groups, time spent immobile was compared.

### 2.11.5. Rotarod test

The rotarod test was performed to evaluate the balance and motor coordination. The animals were placed on a rotating rod that rotates at a speed ranging from 1 to 4 revolutions per minute. The test was completed when the mouse fell off the rod and landed on the sponge bed that was kept at the base of the apparatus. Parameters such as total time spent by the animals on the rod and the distance traveled by them were quantified and compared between the two groups.

## 2.12. Statistical analysis

GraphPad Prism 9, Microsoft Excel, and Python were used for all data and statistical analyzes in this study. For image analysis ImageJ/Fiji was used. The data is presented as cumulative distributions and Mean  $\pm$  SEM. To determine the *p*-values and test for statistical significance, we used the Kolmogorov–Smirnov test (K-S test), student's *t*-test (Normally distributed data determined using Shapiro–Wilk test), Mann–Whitney test (Non-normally distributed data), one-way and two-way ANOVA, and associated post-hoc tests.

## 3. Results

### 3.1. Generation of ACE2 KO mice using CRISPR-Cas9 genome editing tools

The olfactory system of rodents is an attractive model to study the circuit mechanisms of many brain dysfunctions. The well-mapped anatomical organization, the ease of accessibility of different olfactory centers, and olfaction being the dominant sensory modality of rodents make it an efficient tool to modulate circuit functions which give rise to specific behavioral phenotypes mimicking brain disorders. Since the beginning of pandemic, olfactory system remained as the most studied sensory system due to prevalent olfactory and cognitive dysfunctions caused by SARS CoV-2 infection. As ACE2 receptor was one of the molecular factors mediating the virus entry (Klingenstein et al., 2020), ACE2 KO mouse model was generated using CRISPR-Cas9 by deleting the translation start site of the exon 2 of the ACE2 gene (Figure 1A). Guide RNAs for 5' and 3' end of the targeted region were chosen to generate the knockout. The mouse zygote was microinjected with the transcribed gRNA/Cas9 mRNAs, after the vectors that target ACE2 gene deletion were constructed using the guide RNAs. For confirmation of the deletion, the genomic DNA of

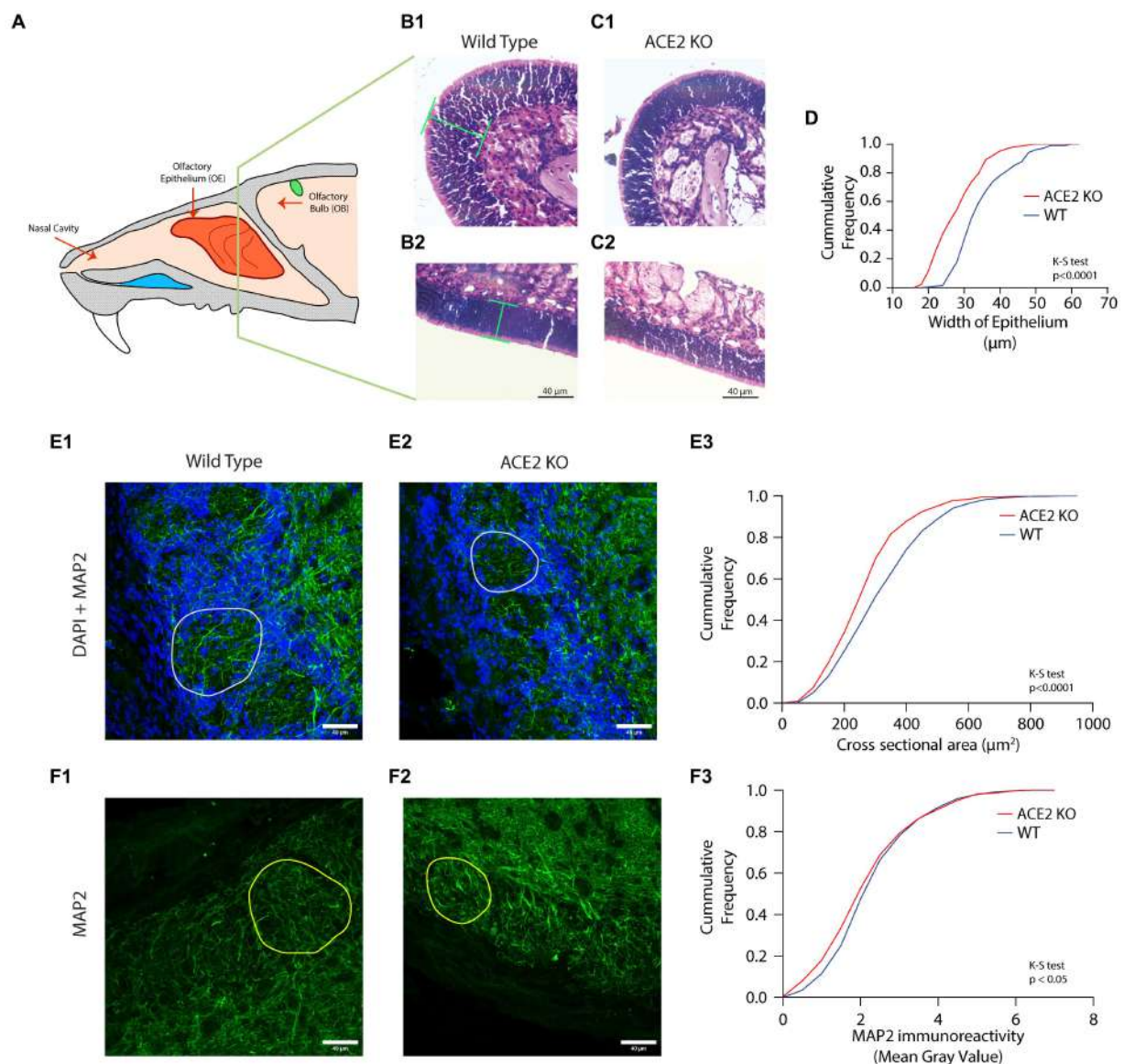


FIGURE 2

Morphological aberrations in the olfactory epithelium (OE) and olfactory bulb (OB) of ACE2 KO animals. **(A)** Schematic representation of the mouse olfactory system. The olfactory epithelium (OE) is present in the posterior region of the nasal cavity and harbors olfactory sensory neurons (OSNs). These OSNs express odor receptors. The signal from the OSNs is then transduced to the olfactory bulb (OB). **(B,C)** Representative images of different regions of OE stained with Hematoxylin and Eosin for WT **(B1,B2)** and ACE2 KO **(C1,C2)** animals, respectively. Green lines in the panel **B1** and **B2** represent the width of the epithelium. **(D)** Cumulative frequency distribution of epithelium width for ACE2 KO and WT animals. The width of epithelium for WT was  $35.39 \pm 0.5294 \mu\text{m}$ , ACE2 KO:  $28.67 \pm 0.4408$ , K-S test,  $p < 0.0001$ , number of animals:  $n_{\text{WT}} = 4$  and  $n_{\text{ACE2 KO}} = 4$ , number of region of interests (ROI): WT=211, ACE2 KO=232. **(E)** Representative images of the glomerular layer of the OB stained with DAPI and MAP2 from WT **(E1)** and ACE2 KO animals **(E2)**. DAPI is visualized with blue color, whereas MAP2 is visualized with green color. **(E3)** Cumulative frequency distributions of cross-sectional area of the glomeruli pooled for WT and ACE2 KO animals. The cross-sectional area for WT was  $335.6 \pm 6.444 \mu\text{m}^2$ , for ACE2 KO was  $283.1 \pm 5.191 \mu\text{m}^2$  (K-S test,  $p < 0.0001$ , number of animals:  $n_{\text{WT}} = 3$  and  $n_{\text{ACE2 KO}} = 3$ , number of glomeruli: WT=496, ACE2 KO=558). **(F)** Representative images of the glomerular layer of the OB stained with MAP2 (green) for WT **(F1)** and ACE2 KO animals **(F2)**. Yellow colored circles in the images represent individual glomeruli. **(F3)** Cumulative frequency distributions of MAP2 immunoreactivity measured using mean intensity for WT and ACE2 KO animals. The MAP2 immunoreactivity for WT was  $2.490 \pm 0.0499$ , for ACE2 KO was  $2.357 \pm 0.0517$  (K-S test,  $p = 0.0349$ , number of animals:  $n_{\text{WT}} = 3$  and  $n_{\text{ACE2 KO}} = 3$ , number of glomeruli: WT=496, ACE2 KO=558).

the F0 mice was subjected to the PCR and was visualized using agarose gel electrophoresis. A shorter PCR product of the expected size was visible on the agarose gel. Visualization of the agarose gel revealed deletions in samples 4, 5, 9, and 10 with sample 10 showing the maximum deletion (band shown in sample 10 of Figure 1B). The deletions were further confirmed by performing the sequencing for samples 5 and 10 in which 84bp and 246bp deletions were observed,

respectively, (Figure 1C). F0 female mouse (sample 10) was further crossed with C57 BL6 males and the progenies were then backcrossed for three generations to obtain enough number of homozygous KO animals. The genotype of experimental mice were further confirmed by western blotting to check the ACE2 protein levels in the brains of ACE2 KO and WT animals. In contrast to WT animals, which showed prominent bands for ACE2, western blot analysis did not reveal any

band corresponding to ACE2 protein in the ACE2 KO animals. Bands for GAPDH, which acted as an internal control, were observed in both groups of animals (Figure 1D), thereby confirming the absence of ACE2 proteins in the brains of animals used in the experiments. These results therefore confirm the successful generation of the ACE2 KO mouse model. Further, morphological phenotypes of these mice were assessed using microscopic techniques and the behavioral phenotypes were studied using various assays.

### 3.2. ACE2 KO animals exhibit morphological alterations in the olfactory epithelium and olfactory bulb

Although there are mouse models available to study underlying mechanisms of brain dysfunctions caused by SARS CoV-2 infection, a detailed characterization of sensory as well as cognitive deficits using precise behavioral assays are lacking to date. In the olfactory system of rodents, ACE2 receptors are primarily found in supporting sustentacular cells of the olfactory epithelium (Bilinska et al., 2020; Butowt and Bilinska, 2020; Lechien et al., 2021). Due to the protective and supporting nature of sustentacular cells, the viral infection resulting in the internalization of receptors can cause neuroinflammatory changes leading to gradual decaying of OSN functions. To investigate the effect of ACE2 receptor knockout on the morphology of OSNs, we first quantified the OSN layer thickness and compared it to that of wildtype (WT) mice (Figure 2A). Coronal sections of the OE stained with Hematoxylin and Eosin were used to measure the OE thickness, which was assessed as the perpendicular distance from the basal membrane. For ACE2 KO, 232 regions of interest (ROIs), and for WT mice, 211 ROIs were analyzed along anterior–posterior and mediolateral axes for four mice in each group. The cumulative distributions of epithelium width measurements reveal smaller OE thickness in ACE2 knockout mice in comparison to that of the WT animals, indicating the role of supporting cells in maintaining the morphology of the OE (Figures 2B–D, WT:  $35.39 \pm 0.5294 \mu\text{m}$ , ACE2 KO:  $28.67 \pm 0.4408$ , K-S test,  $p < 0.0001$ ). In addition, we measured the epithelial thickness in different areas near to the septum (henceforth named as septal areas, dorsomedial and middle meatus areas) and other turbinate regions toward lateral side (ethmoturbinate areas) in each section, with similar numbers from both locations. On analyzing these areas separately, we observed lower thickness of olfactory epithelium in ACE2 KO animals in both locations, thereby confirming that reduction in epithelium thickness is independent of the location on the turbinates (Supplementary Figure S1, ACE2 KO vs. WT: K-S test,  $p < 0.0001$  for both septal and ethmoturbinate areas).

The OSNs project to glomeruli of OB in a receptor specific manner. In the glomeruli, these OSNs makes synapses with the Mitral/ Tufted cells, which are the output neurons of the OB. Since the morphological characteristics of OB glomeruli are dependent on the axonal inputs of OSNs (Potter et al., 2001), we hypothesized that the reduction observed in the OE thickness may result in the alterations of glomeruli morphology. To accomplish this, a quantitative analysis of the cross-sectional area of individual glomeruli was performed across ACE2 KO (558 glomeruli) and WT mice (496 glomeruli). The cumulative frequency distribution of the glomeruli area revealed a reduction in the cross-sectional area of olfactory glomeruli in ACE2

KO mice compared to WT, C57BL/6J animals (Figures 2E1–E3, WT:  $335.6 \pm 6.444 \mu\text{m}^2$ , ACE2 KO:  $283.1 \pm 5.191 \mu\text{m}^2$ , K-S test,  $p < 0.0001$ ). In addition to the cross-sectional area, we also analyzed the perimeter and minimum and maximum diameter. The perimeter and minimum and maximum diameter for glomeruli of the ACE2 KO animals were lower than that of the WT animals (Supplementary Figure S2). Further, to investigate the potential modifications in the neural circuits caused by the knockout of ACE2 receptors, we performed the immunostaining for the neuronal cytoskeletal protein MAP2, which stains the neurites. The qualitative analysis revealed a more prominent and discernible neurite projections in the glomeruli of WT animals. To quantify these changes, we calculated the mean gray value corresponding to MAP2 immunoreactivity in individual glomeruli of ACE2 and WT animals. A total of 558 glomeruli in ACE2 KO mice and 496 glomeruli in WT animals were analyzed and the cumulative distribution of intensities were compared across WT and ACE2 KO animals. This quantification revealed significantly lower MAP2 immunoreactivity in ACE2 KO compared to control mice implying severe alterations in neural circuits caused by the knockout of ACE2 receptors (Figures 2F1–F3, WT:  $2.490 \pm 0.0499$ , ACE2 KO:  $2.357 \pm 0.0517$ , K-S test,  $p = 0.0349$ ). Taken together, these results prove morphological aberrations in the sensory periphery (OE) as well as in the pre-cortical sensory area (OB) of ACE2 KO mice, which may cause alterations in the sensory and cognitive abilities of animals.

### 3.3. Altered odor detection and discrimination behavior in ACE2 KO mice

Having observed the morphological aberrations in ACE2 KO mice, we next asked how these aberrations are affecting their olfactory behavioral readouts. In asymptomatic carriers and symptomatic COVID-19 patients, we have observed compromised odor detection abilities more strikingly at the threshold levels (Bhattacharjee et al., 2020; Pardasani and Abraham, 2022; Bhowmik et al., 2023). Therefore, we investigated the detection abilities of ACE2 KO and WT mice using different batches of animals by training them on a go/no-go operant conditioning paradigm using different concentrations of specific odors vs. mineral oil (MO). On training mice to discriminate Methyl Benzoate from MO, ACE2 KO mice did not show any difference in the learning pace compared to WT animals (Figure 3A; MB,  $10^{-10}\%$ ,  $10^{-8}\%$ , and  $10^{-6}\%$ , diluted in MO, two-way ANOVA for each concentration, non-significant (ns) represents  $p > 0.05$ ). However, ACE2 KO mice showed slower learning pace for certain concentrations on training them to discriminate (+) Limonene ( $10^{-10}\%$ ,  $10^{-9}\%$ , and  $10^{-8}\%$ ) from MO (Figure 3B, two-way ANOVA for each concentration, \* represents  $p < 0.05$  and ns represents  $p > 0.05$ ). As these alterations can be dependent on the odorants used, a detailed screening using many odor pairs and more concentrations will be required to find out the changes in odor detectabilities.

As we observed varying detection abilities with ACE2 KO, we further studied odor discriminations using a complex binary mixture of Amyl acetate (AA) and Ethyl butyrate (EB) at varying concentrations (see methods). We quantified and compared various behavioral readouts from KO and WT animals to confirm the behavioral phenotypes caused by the knockout of ACE2 receptors. KO mice showed slower learning pace compared to control animals at different concentrations (Figure 3C, two-way ANOVA for each



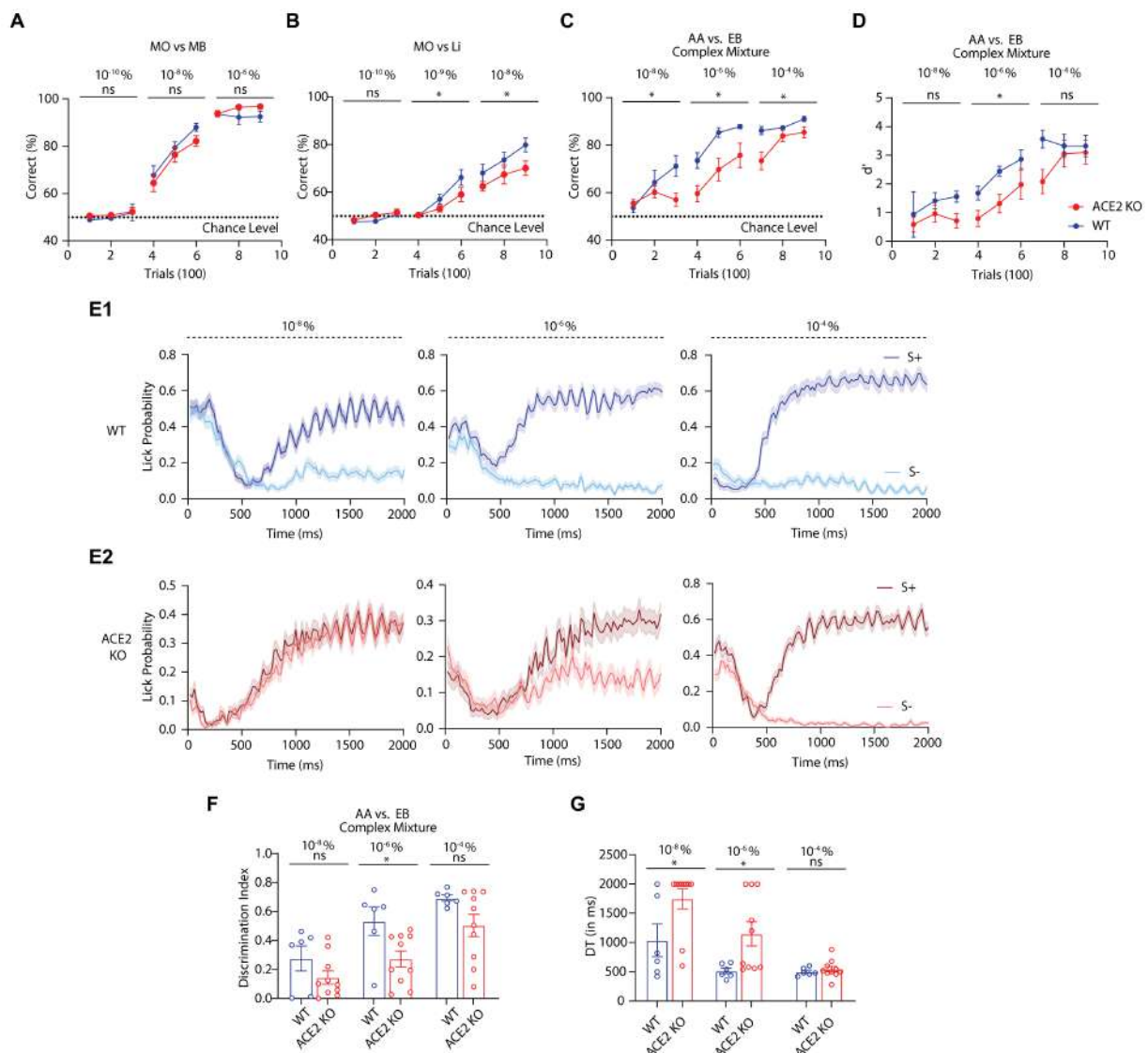


FIGURE 3

Odor detection and discrimination characteristics of WT and ACE2 animals. **(A)** Accuracy of performance shown by learning curves for WT and ACE2 KO animals when trained to discriminate mineral oil (MO) vs. Methyl Benzoate (MB) at different concentrations ( $10^{-10}\%$ ,  $10^{-8}\%$ , and  $10^{-6}\%$ ). Comparisons of learning curves: Two-Way ANOVA. For,  $10^{-10}\%$ : [ $F(1,45)=0.8053$ ,  $p=0.3743$ ],  $10^{-8}\%$ : [ $F(1,45)=2.495$ ,  $p=0.1212$ ], and  $10^{-6}\%$ : [ $F(1,45)=4.236$ ,  $p=0.0554$ ], number of animals:  $n_{ACE2KO}=10$ ,  $n_{WT}=7$ . **(B)** Learning curves of WT and ACE2 KO animals for mineral oil (MO) vs. Limonene (+) (Li) at different concentrations ( $10^{-10}\%$ ,  $10^{-8}\%$ , and  $10^{-6}\%$ ). Comparisons of learning curves: Two-Way ANOVA. For,  $10^{-10}\%$ : [ $F(1,66)=3.451$ ,  $p=0.0677$ ],  $10^{-8}\%$ : [ $F(1,63)=4.435$ ,  $p=0.0392$ ], and  $10^{-6}\%$ : [ $F(1,63)=7.574$ ,  $p=0.0077$ ], number of animals:  $n_{ACE2KO}=11$ ,  $n_{WT}=13$ . **(C)** Learning curves of WT and ACE2 KO for a complex odor discrimination task [60% Amyl acetate (AA)+40% Ethyl Butyrate (EB) vs. 60% EB+40% AA, at different concentrations ( $10^{-8}\%$ ,  $10^{-6}\%$ , and  $10^{-4}\%$ ). Comparisons of learning curves: Two-Way ANOVA. For,  $10^{-8}\%$ : [ $F(1,42)=4.605$ ,  $p=0.0377$ ],  $10^{-6}\%$ : [ $F(1,42)=15.09$ ,  $p=0.0004$ ], and  $10^{-4}\%$ : [ $F(1,42)=10.09$ ,  $p=0.0028$ ], number of animals:  $n_{ACE2KO}=10$ ,  $n_{WT}=6$ . **(D)**  $d'$  (d prime) of WT and ACE2 KO animals measured during a complex odor discrimination task, same as panel C, at different concentrations ( $10^{-8}\%$ ,  $10^{-6}\%$ , and  $10^{-4}\%$ ).  $d'$  were compared between WT and ACE2 KO animals using Two-Way ANOVA. For,  $10^{-8}\%$ : [ $F(1,42)=3.360$ ,  $p=0.0739$ ],  $10^{-6}\%$ : [ $F(1,42)=9.663$ ,  $p=0.0034$ ], and  $10^{-4}\%$ : [ $F(1,42)=3.277$ ,  $p=0.0774$ ], number of animals:  $n_{ACE2KO}=10$ ,  $n_{WT}=6$ . **(E)** Lick patterns of WT (**E1**) and ACE2 KO (**E2**) animals for different concentrations during the complex odor discrimination used in panel C and D. Y-axis represents the lick probability as a function of time (X-axis). **(F)** Discrimination index calculated using the lick probabilities at different concentrations. Comparison using two-tailed unpaired t-test: For,  $10^{-8}\%$ :  $p=0.1585$ ,  $10^{-6}\%$ :  $p=0.0235$ , and  $10^{-4}\%$ :  $p=0.5276$ . Number of animals:  $n_{ACE2KO}=10$ ,  $n_{WT}=6$ . **(G)** Comparison of discrimination times (DT) shown by WT and ACE2 KO animals for different concentrations, using two-tailed unpaired t-test: For,  $10^{-8}\%$ :  $p=0.0369$ ,  $10^{-6}\%$ :  $p=0.0367$ , and  $10^{-4}\%$ :  $p=0.0858$ . Number of animals:  $n_{ACE2KO}=10$ ,  $n_{WT}=6$ . In the figure \* indicates  $p<0.05$ , ns indicates: non-significant.

concentration, \* represents  $p<0.05$ ). To account for the hit and false alarm probabilities while learning the discrimination task, d-prime ( $d'$ ) was calculated for both KO and WT groups and significant differences were observed (Figure 3D, two-way ANOVA for each concentration, \* represents  $p<0.05$  and ns represents  $p>0.05$ ).

Further, on analyzing the lick behavior with high temporal precision, we observed the differences in their licking responses toward rewarded and non-rewarded odors (Figures 3E1,E2, see methods). Therefore, we calculated the discrimination index based on this and found significant differences between KO and WT groups (Figure 3F, see

methods, two-tailed unpaired *t*-test for each concentration, \* represents  $p < 0.05$  and ns represents  $p > 0.05$ ). Further, the difference in the reaction times, quantified by discrimination times (DT, see methods), showed slower times for the KO compared to control mice (Figure 3G, two-tailed unpaired *t*-test for each concentration, \* represents  $p < 0.05$  and ns represents  $p > 0.05$ ). In summary, this detailed behavioral phenotyping confirms the olfactory sensory and cognitive deficits due to the knockout of ACE2 receptors.

### 3.4. Impaired novel odor discrimination in ACE2 KO mice

Olfactory dysfunctions are reported as early symptoms in Parkinson's disease (PD) patients (Barresi et al., 2012; Doty, 2012; Fullard et al., 2017; Marin et al., 2018). In addition, a few cases of PD associated with COVID-19 infection have been reported (Li et al., 2020; Sulzer et al., 2020; Merello et al., 2021). As olfactory deficits and PD are strongly linked, we decided to test ACE2 KO mice on a habituation and novel odor discrimination task that is used to phenotype PD mouse models (Fleming et al., 2008; Lehmkuhl et al., 2014). Animals' ability to discriminate between a familiar odor and a novel odor was assessed by quantifying the time spent by them to sample the new odor after getting exposed to another stimulus (familiar odor) few times. In brief, mice were exposed to an odor for 3 min on one side of a cage while the opposite side had similar box without any odor. They were exposed five times rotating the cage 180 degrees for each trial (Figure 4A). The novel odor discrimination was assessed by comparing the time spent by animals in sampling the novel odor vs. the habituated odor. While WT mice spent a significantly longer time for exploring the novel odor compared to the habituated odor (Figure 4B, Habituated odor:  $3.753 \pm 0.7959$  s, Novel odor:  $6.908 \pm 1.514$  s, one-tailed paired *t*-test,  $p = 0.0132$ ), ACE2 KO animals spent a similar amount of time exploring both the odors (Figure 4C, Habituated odor:  $3.449 \pm 0.6708$  s, Novel odor:  $4.743 \pm 0.9469$  s, one-tailed paired *t*-test,  $p = 0.0965$ ). Hence, our results revealed impairments in novel olfactory discriminations in animals with knockout of ACE2 receptors.

### 3.5. ACE2 KO female mice display compromised multimodal pheromonal location memory

Rodent olfactory subsystems can process various types stimuli including pheromones. Volatile components of pheromones have been shown to be processed by main olfactory bulb (MOB) (Buck, 2000). As we observed morphological aberrations in the MOB, we studied the pheromone detection abilities of ACE2 KO mice. When presented with pheromonal cues from the opposite sex in form of the soiled bedding, sexually mature ACE2 KOs and control female mice explored these cues in a similar manner. This was quantified by measuring the time spent near to the soiled bedding kept at the center of an open arena (Figures 5A1-A4, WT:  $118.8 \pm 17.06$  s, ACE2 KO:  $138.8 \pm 26.19$  s, two-tailed unpaired *t*-test,  $p = 0.5143$ ). This result shows similar pheromonal detection abilities in ACE2 KO and control animals.

In nature, pheromone location information helps animals finding their mates and avoiding potential predators. This information can

also be carried by the substances where the semiochemicals are being sprayed. Therefore, involvement of whiskers along with the olfactory system is anticipated in enabling the multimodal association between pheromones and their locations. Hence, we investigated whether ACE2-KO mice show any deficits in the acquisition of this multimodal information. We employed an established behavioral paradigm to quantify the multimodal learning of pheromonal locations (Pardasani et al., 2021). When mice were allowed to explore both pheromone and neutral stimulus containing chambers (which were closed with lids having holes of different diameters, see Materials and Methods for the details, Figures 5B1,B2) in a three-chambered assay, no consistent preferences toward either of these chambers were observed. Both groups spent time in front of the chamber and displayed active attempts in sampling pheromonal cues, confirming their detection abilities (Figures 5C1-D2, two-way ANOVA with Bonferroni's multiple comparison test for time spent and number of active attempts for both groups of animals, \* represents  $p < 0.05$  and ns represents  $p > 0.05$ ). Both groups of mice were then trained for 15 days to associate pheromonal cues with varying orifice' diameters on the lid of the respective chambers (see methods). Their memory of multimodal association was assessed 15 days after the completion of training. The time spent in front of the urine chamber and the number of active attempts for sampling pheromonal cues were used to calculate the corresponding memory index. ACE2 KO females exhibited significantly lower memory index compared to the WT animals (Figures 5E1-F2, Memory index; Time Spent, WT:  $2.002 \pm 0.5185$ , ACE2 KO:  $0.4774 \pm 0.2123$ , two-tailed unpaired *t*-test,  $p = 0.0483$ ; Number of active attempts, WT:  $2.118 \pm 0.54$ , ACE2 KO:  $0.7249 \pm 0.5810$ , two-tailed Mann-Whitney test,  $p = 0.0186$ ). These results imply impaired cognitive abilities caused by the knockout of ACE2 receptors.

### 3.6. ACE2 KO mice did not display any anxiety or depression phenotypes

Having observed sensory as well as cognitive deficits in ACE2 KO mice, we further studied if these phenotypes were triggered by any anxiety-related or depressive behaviors that might be caused by the knockout of ACE2 receptors. This study was also prompted by the observations of long-term sensory and cognitive deficits (Bhattacharjee et al., 2020; Bhowmik et al., 2023) and mood disorders (Lamontagne et al., 2021) reported during and post-COVID conditions. We employed an array of commonly used behavioral paradigms to quantify these behaviors (Belovicova et al., 2017). On conducting open field test with experimental and control groups of mice, we did not observe any differences between the groups in the number and latency of entries to the center and the time spent in the center and the corners of the field (Figures 6A1-A4, two-tailed unpaired *t*-test for each parameter, ns represents  $p > 0.05$ ). In the elevated plus, we did not observe any differences in the time spent and number of entries in the open and closed arms (Figures 6B1-B4, two-tailed unpaired *t*-test for each parameter, ns represents  $p > 0.05$ ). These results indicate the absence of any anxiety-related behaviors due to the knockout of ACE2 receptors. To test for any depressive phenotypes, we conducted tail suspension and forced swim tests. Time of immobility was not different between the control and knockout groups of mice in the tail suspension test (Figure 6C, two-tailed



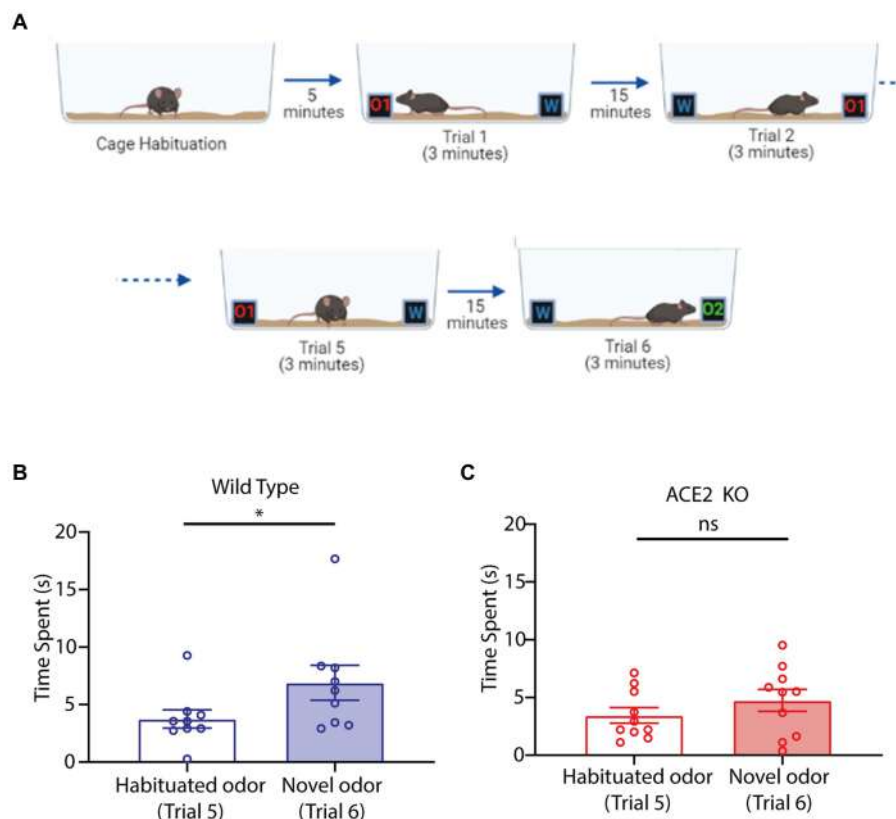


FIGURE 4

Novel odor discrimination is impaired in ACE2 KO animals. (A) Schematic of the novel discrimination task. The task begins with animals getting habituated with the cage followed by 5 trials of odor habituation wherein at one end an odorant (O1) was provided whereas on the other end there was water (W). For each trial the cage was rotated by 180° to mitigate any non-specific preference. Following habituation, the odor O1 was replaced by a novel odor (O2) and time spent by animals near the novel odor (Trial 6) vs. habituated odor (Trial 5) was used to assess the novel odor discrimination ability. (B) Comparison of time spent by WT animals during the task near the habituated and the novel odor. Time spent by animals near habituated odor ( $3.753 \pm 0.7959$ s) was significantly lower than that for novel odor ( $6.908 \pm 1.514$ s), one-tailed paired *t*-test,  $p = 0.0132$ ,  $n = 9$ . (C) Comparison of time spent by ACE2 KO animals during the task near the habituated and the novel odor. Time spent by animals near habituated odor ( $3.449 \pm 0.6708$ s) and novel odor ( $4.743 \pm 0.9469$ s) was similar, one-tailed paired *t*-test,  $p = 0.0965$ ,  $n = 10$ .

unpaired *t*-test,  $p = 0.3374$ ). In the forced swim test, immobility was slightly higher for the WT group, indicating the absence of any depressive symptoms in ACE2 KO mice (Figure 6D, two-tailed unpaired *t*-test,  $p = 0.0264$ ). Further, we carried out the rotarod test to see if there are any motor deficits in ACE2 KO mice and time spent on the rotarod and the distance covered by both groups of animals were found to be similar (Figures 6E1,E2, two-tailed unpaired *t*-test, ns represents  $p > 0.05$ ), indicating the absence of any motor dysfunctions due to the knockout of ACE2 receptors. All these tests provide the evidence for the absence of any mood disorder-related phenotypes in ACE2 knockout mice. Taken together, our results prove sensory and cognitive deficits in ACE2 KO mouse model, supported by the morphological aberrations we observed in these mice.

## 4. Discussion

Neurological complications of long-COVID may challenge the global health for many more years (Kay, 2022). Various olfactory problems including hyposmia, anosmia, and parosmia have been reported during infection and under long-COVID conditions (Bhattacharjee et al., 2020; Pardasani and Abraham, 2022; Bhowmik

et al., 2023). While infection at the olfactory periphery and the neuronal loss may explain the transient hyposmic and anosmic conditions, parosmia may result from the mis-targeting of regenerating OSNs during the recovery period (Costanzo, 2000; John and Key, 2003; Cooper et al., 2020). The expression of ACE2 receptors, that mediates virus infection in sustentacular cells of olfactory epithelium, explains the severe olfactory problems under COVID-19 infection. Therefore, we aimed to generate a complete ACE2 knockout mouse model using the CRISPR-Cas9 based genome editing method and investigate its function in modulating olfactory information processing. The deletion of ACE2 receptors may not lead to all pathophysiological conditions caused by SARS-CoV2 infection. However, the loss of ACE2 receptor function in the supporting sustentacular cells may ultimately result in the ionic imbalance in the epithelium, causing the cell death of olfactory sensory neurons, hence leading to various olfactory dysfunctions (Cooper et al., 2020).

Transgenic models can be created by different approaches. For example, in Cre-Lox recombination system, the expression specificity is achieved by crossing floxed mouse lines with Cre driver lines or by delivering Cre recombinase in a cell type-specific manner (Capecchi, 2005; Taniguchi et al., 2011). The generation of these mouse lines takes

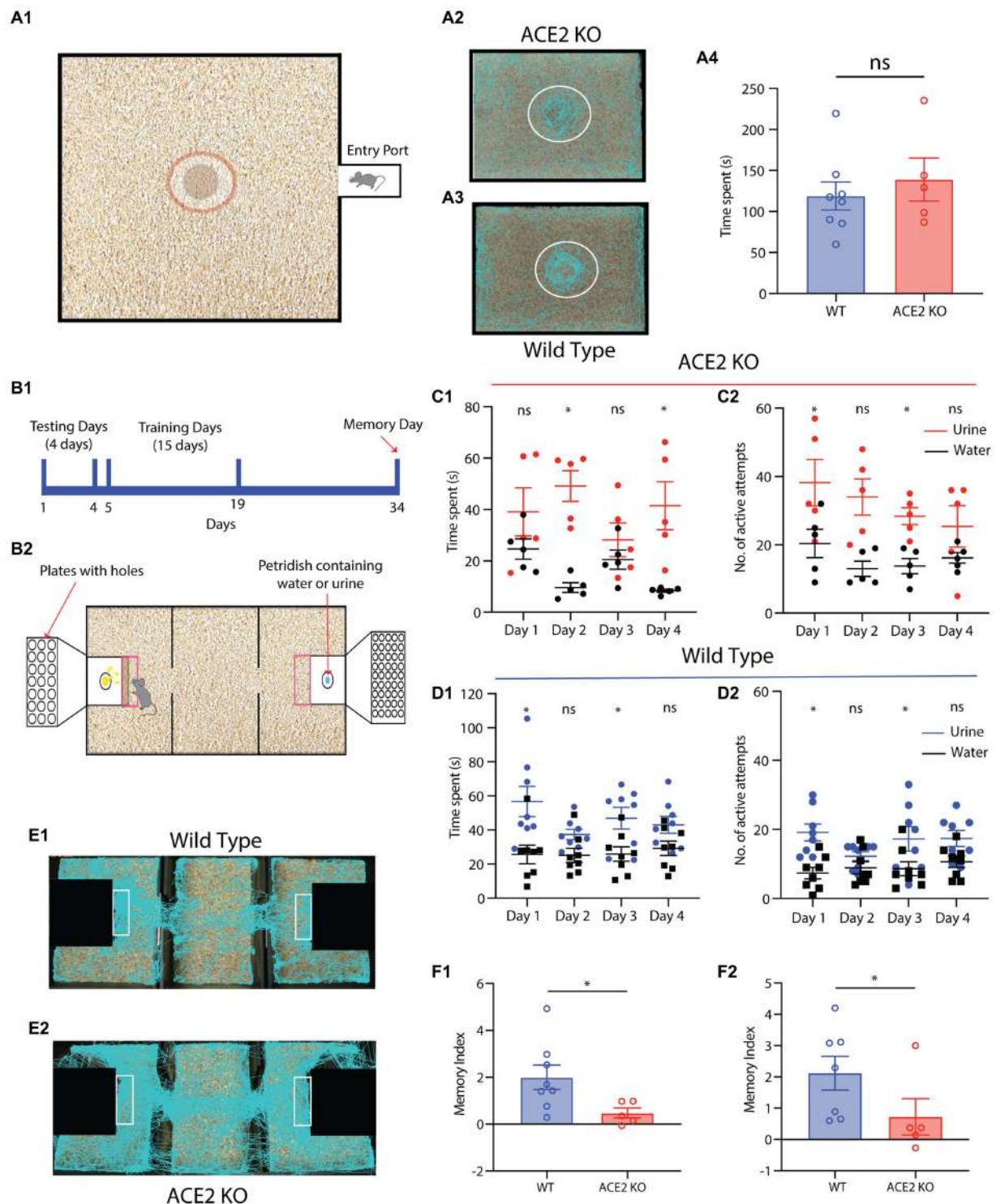


FIGURE 5

ACE2 KO animals show impaired memory in a multimodal pheromone learning task. **(A)** Pheromone detection abilities of ACE2 KO animals are similar to that of the WT animals. **(A1)** Diagrammatic representation of the setup used for pheromonal detection assay. The dimensions of the setup are 60cm x 45cm. A petri dish containing male soiled bedding and urine was placed at the center of the arena and females were introduced in this arena. The animals were tracked using EthoVision software while their motions were captured on camera. The time spent by females near to the petri dish was measured in order to gauge their pheromonal detection abilities. **(A2,A3)** Representative tracks taken by ACE2 KO and WT animals during the pheromone detection task, respectively. **(A4)** The pheromonal detection abilities of both groups of the animals was similar (WT:  $118.8 \pm 17.06$ s, ACE2 KO:  $138.8 \pm 26.19$ s, two-tailed unpaired *t*-test,  $p = 0.5143$ ,  $n_{ACE2KO} = 5$ ,  $n_{WT} = 8$ ). **(B)** **(B1)** Timeline of multimodal pheromone location learning task. Animals undergo testing for first 4 days, followed by 15 days training. Fifteen days post completion of the training, the memory of the animals was assessed. **(B2)** Illustration of the setup used for training the animals to associate the urine smell and neutral stimuli with specific orifice diameters. **(C,D)** Sampling parameters of ACE2 KO and Wildtype (WT) animals during first 4 days of testing, respectively. **(C1)** Time spent by ACE2 KO females near the water and urine zone during the testing days (two-way ANOVA with Bonferroni's multiple comparison test, \* represents  $p < 0.05$  and ns represents  $p > 0.05$ ). **(C2)**

(Continued)

FIGURE 5 (Continued)

Number of active attempts by ACE2 KO females near the water and urine zone during the testing days (two-way ANOVA with Bonferroni's multiple comparison test, \* represents  $p < 0.05$  and ns represents  $p > 0.05$ ,  $n_{ACE2KO} = 5$ ). (D) (D1) Time spent by WT females near the water and urine zone during the testing days (two-way ANOVA with Bonferroni's multiple comparison test, \* represents  $p < 0.05$  and ns represents  $p > 0.05$ ). (D2) Number of active attempts by WT females near the water and urine zone during the testing days (two-way ANOVA with Bonferroni's multiple comparison test, \* represents  $p < 0.05$  and ns represents  $p > 0.05$ ,  $n_{WT} = 8$ ). (E) (E1,E2) Representative tracks during the memory day for WT and ACE2 KO animals, respectively. (F) Comparison of Memory index between ACE2 KO and WT animals calculated using time spent and the number of active attempts. (F1) ACE2 KO females showed impaired memory (index calculated using time spent) compared to the WT animals (WT:  $2.002 \pm 0.5185$ , ACE2 KO:  $0.4774 \pm 0.2123$ , two-tailed unpaired  $t$ -test,  $p = 0.0483$ ). (F2) ACE2 KO females showed impaired memory (index calculated using number of active attempts) compared to the WT animals ( $2.118 \pm 0.54$ , ACE2 KO:  $0.7249 \pm 0.5810$ , two-tailed Mann–Whitney test (non-normal distribution),  $p = 0.0186$ ,  $n_{ACE2KO} = 5$ ,  $n_{WT} = 7-8$ ).

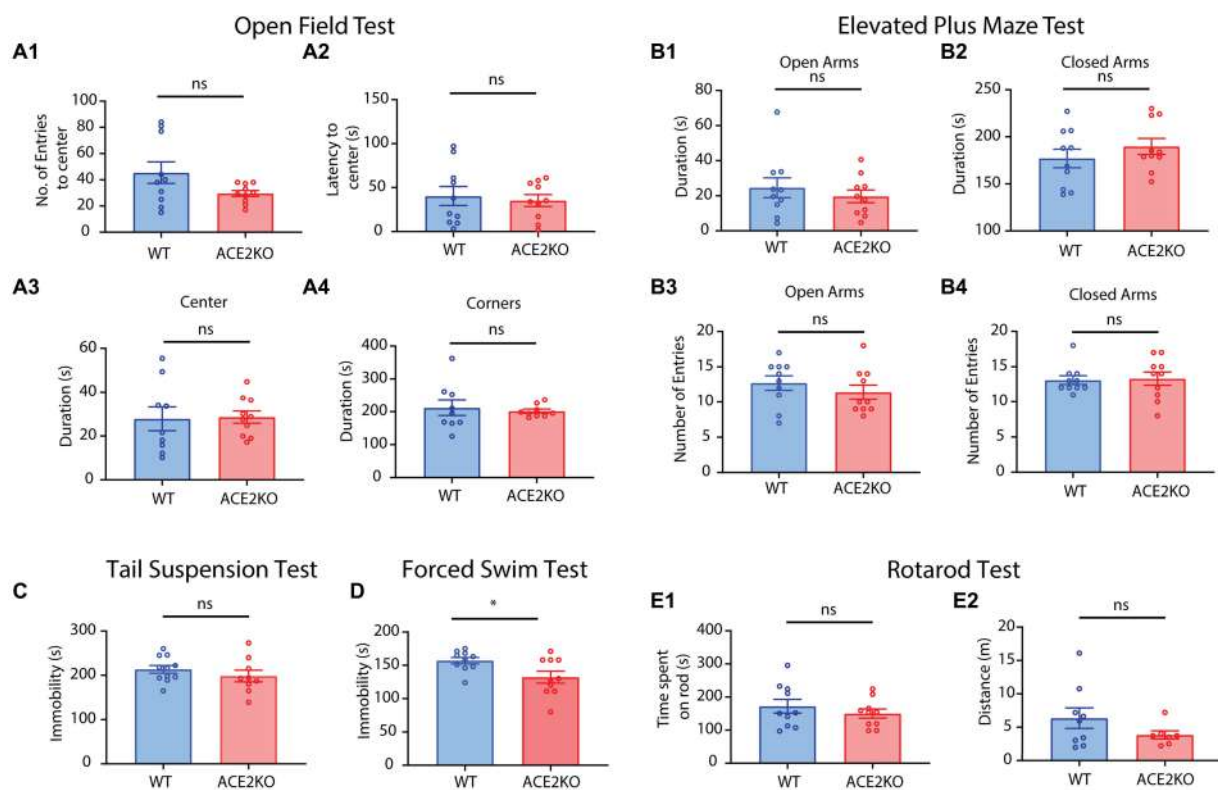


FIGURE 6

ACE2 KO and WT animals showed no differences in mood disorder-related behaviors. (A) Comparison of different parameters between ACE2 KO and WT animals for an open field test (OFT). (A1) Number of entries to the center between WT ( $45.40 \pm 8.224$ ) and ACE2 KO ( $29.50 \pm 2.296$ ) animals was similar (two-tailed unpaired  $t$ -test,  $p = 0.0790$ ). (A2) Latency to the center between WT ( $40.34 \pm 10.83$ s) and ACE2 KO ( $35.17 \pm 6.170$ ) animals was similar (two-tailed unpaired  $t$ -test,  $p = 0.6895$ ). (A3) Time spent in the center between WT ( $27.81 \pm 5.448$ s) and ACE2 KO ( $28.60 \pm 2.825$ ) animals was similar (two-tailed unpaired  $t$ -test,  $p = 0.8953$ ). (A4) Time spent in the corners between WT ( $212.0 \pm 23.80$ s) and ACE2 KO ( $201.5 \pm 6.158$ s) animals was similar (two-tailed unpaired  $t$ -test,  $p = 0.6774$ ). Number of animals:  $n_{ACE2KO} = 10$ ,  $n_{WT} = 9-10$ . (B) Comparison of different parameters between ACE2 KO and WT animals for an elevated plus maze test (EPM). (B1) Time spent in open arms between WT ( $177.1 \pm 9.792$ s) and ACE2 KO ( $189.8 \pm 8.491$ ) animals was similar (two-tailed unpaired  $t$ -test,  $p = 0.3403$ ). (B2) Time spent in closed arms between WT ( $177.1 \pm 9.792$ s) and ACE2 KO ( $189.8 \pm 8.491$ ) animals was similar (two-tailed unpaired  $t$ -test,  $p = 0.4747$ ). (B3) Number of entries in open arms between WT ( $12.70 \pm 1.023$ ) and ACE2 KO ( $11.40 \pm 1.013$ ) animals was similar (two-tailed unpaired  $t$ -test,  $p = 0.3784$ ). (B4) Number of entries in closed arms between WT ( $12.70 \pm 1.023$ ) and ACE2 KO ( $11.40 \pm 1.013$ ) animals was similar (two-tailed unpaired  $t$ -test,  $p = 0.8615$ ). Number of animals:  $n_{ACE2KO} = 10$ ,  $n_{WT} = 10$ . (C) Comparison of time immobile by ACE2 KO and WT animals for tail suspension test (TST). There was no significant difference in the time spent immobile between the groups (WT:  $213.5 \pm 8.628$ s, ACE2 KO:  $198.4 \pm 13.30$ s, two-tailed unpaired  $t$ -test,  $p = 0.3374$ , number of animals:  $n_{ACE2KO} = 9$ ,  $n_{WT} = 11$ ). (D) Comparison of time spent immobile by ACE2 KO and WT animals for forced swim test (FST). Time immobile by the ACE2 KO animals was significantly higher than that by the WT WT:  $0.1570 \pm 4.798$ s, ACE2 KO:  $132.3 \pm 9.017$ s, two-tailed unpaired  $t$ -test,  $p = 0.0264$ , number of animals:  $n_{ACE2KO} = 10$ ,  $n_{WT} = 10$ . (E) Comparison of different parameters between ACE2 KO and WT animals for rotarod test. (E1) There was no significant difference in the time spent on the rod between the groups (WT:  $172.2 \pm 20.61$ s, ACE2 KO:  $149.9 \pm 13.55$ s, two-tailed unpaired  $t$ -test,  $p = 0.3762$ ). (E2) There was no significant difference in the total distance covered between the groups (WT:  $6.356 \pm 1.544$ m, ACE2 KO:  $3.836 \pm 0.6166$ m, two-tailed unpaired  $t$ -test,  $p = 0.1935$ ).

longer than a year as it requires extensive backcrossing to screen for a homogenous background. The recent advancement in the CRISPR-Cas9 genome editing tools have enabled the researchers to

generate robust mouse models with targeted genetic background comparatively faster (Nishizono et al., 2020). The knockouts and knockins can be directly generated by injecting the guide RNA and



Cas9 into the pronucleus of fertilized mouse eggs (Yang et al., 2013). The existing ACE2 knockout mouse models created with CRISPR-Cas9 were mostly used to study the pulmonary and cardiovascular systems, and differences in knockout phenotypes are being reported. The genetic make-up of the models may attribute to the inconsistencies of the observed phenotypes, which can be considered as a drawback of the CRISPR-Cas9 approach (Jia et al., 2020). In this study, the deletion of ACE2 gene was ensured by targeting the crucial translational start site of the exon 2 and was confirmed by sequencing and western blotting.

The COVID-19 pandemic struck the world recording a high mortality rate and causing a decrease of human wellbeing globally. Since the start of the pandemic, numerous studies have been conducted to identify the various entry routes of SARS-CoV-2. The human angiotensin-converting enzyme 2 (hACE2) receptor was confirmed to be the target of the spike glycoprotein of the virus (Whittaker et al., 2021). After the viral glycoprotein binds to the ACE2 receptor, the TMPRSS2 protein cleaves the virus' S2 site, causing the internalization of the virus (Glowacka et al., 2011; Jackson et al., 2022). The widespread expression of ACE2 receptors indicates toward number of possible entry points for the invasion of virus (Mainland et al., 2015; Sungnak et al., 2020; Zhou et al., 2020; Boldrini et al., 2021; Casagrande et al., 2021; Huang N. et al., 2021; Pardasani and Abraham, 2022). Additionally, the virus can also enter the body through a breach of the blood-brain barrier (BBB), which is caused by the instability of the barrier by an increase in inflammatory cytokines following infection (Huang X. et al., 2021). Despite the debate over the virus's route of entry, it is recognized to be associated to the ACE2 receptors. As SARS-CoV2 entry into the cells through membrane fusion is thought to down-regulate the ACE2 receptors with a loss of these receptors' catalytic effect (Verdecchia et al., 2020), we created the ACE2 KO mouse model to mimic the effects of COVID-19 and studied its long-term effects. Even though it may not alter organ systems' functions as during or after COVID-19 infection, the ACE2 KO model offers a platform for the exploration of various parameters that can affect overall human well-being as a result of long-COVID-19.

The COVID-19 infection leads to morphological and functional alterations in the brain (Douaud et al., 2022; Du et al., 2023). Since the sustentacular cells of the olfactory epithelium contain the ACE2 receptor, we started by examining the impact of ACE2 deletion on the morphology of the olfactory epithelium (Brann et al., 2020). The width of the epithelium was considerably smaller in the ACE2 KO animals than in the control animals. Additionally, the glomeruli's cross-sectional area and MAP2 immunoreactivity were both reduced in the ACE2 KO animals. These findings demonstrate the changes brought about by the deletion of ACE2 in the olfactory epithelium and olfactory bulb. In humans, COVID-19 has been shown to increase apoptosis and decrease neurogenesis in the hippocampus (Bayat et al., 2022). In mouse models, it has been shown that ACE2 loss causes a reduction in the exercise-induced hippocampal neurogenesis (Klempin et al., 2018; Alenina and Bader, 2019). Given the relationship between ACE2 and COVID-19 and the fact that the olfactory epithelium is another part of the brain where

neurogenesis occurs (Crews and Hunter, 1994), it is probable that the decreased width of the OE is the result of increased apoptosis or reduced neurogenesis. Further studies investigating apoptosis and OSN turnover would be needed to confirm this.

The COVID-19 infection also causes learning and cognitive impairments that even persisted in the post-COVID conditions (Hampshire et al., 2021; Hugon et al., 2022; Bhowmik et al., 2023). Our observations of ACE2 KO animals having deficits in detection, discrimination, and novel odor recognition were similar to clinical observations made in patients. Humans' orbitofrontal cortex has extensive connections to other cortical areas and may help in processing of complex olfactory inputs (McGann, 2017). A decrease in the thickness of gray matter in the orbitofrontal cortex as a consequence of the COVID-19 may also contribute to severe olfactory and cognitive dysfunctions observed in humans (Douaud et al., 2022). In support of these clinical observations, earlier ACE2 KO mouse models exhibited learning impairments in Morris water maze and Y-maze tasks (Wang et al., 2016). In addition, ACE2 activation in the brain has been proven to have protective effects against the cognitive decline caused by amyloid pathology in a mouse model of Alzheimer's Disease (Evans et al., 2020). Despite these supporting evidence, the effect of CRISPR-Cas9 based disruption of ACE2 expression on other gene networks, may not mimic the exact pathophysiological conditions caused by COVID-19 (Stephan et al., 2022).

Rodents' olfaction is critical for their social and reproductive behaviors. During courtship behavior, olfactory system detects pheromones and recognizes their location (Pardasani et al., 2021). Here, we also investigated how ACE2 KO affected the animals' capacity for pheromone detection and the association of pheromones with their location. While the pheromonal detection abilities were unaffected, the ACE2 KO animals displayed poor memory of the pheromone location association, implying the impact of ACE2 deletion on rodents' social and reproductive behaviors. As a result of COVID-19 pandemic, a decline in sexual interest, and frequency were observed (Pascoal et al., 2021). In contrast, a few populations showed an increase in sexual desire, however with a reluctance toward conception (Yuksel and Ozgor, 2020). These findings emphasize the negative impact of the pandemic on human sexual health and success. These problems with reproductive health might be transient and may have resulted by COVID-19's detrimental effects on mental health. According to World Health Organization's assessment, the pandemic caused a 25% rise in the prevalence of anxiety and depression globally (WHO, 2022). However, over time, the behaviors linked to the deterioration of mood disorders such as anxiety and depression was diminishing, suggesting that these effects are transient and may have been attributed to a variety of factors during the pandemic (Manchia et al., 2022). In our analysis of mood disorder related behaviors, ACE2 KO animals did not show any depression or anxiety phenotypes.

In summary, our results demonstrate that knockout of ACE2 receptors leads to sensory and cognitive disabilities, which were similar to clinical observations made from COVID-19 patients. Further, our experimental strategy provides a potential method for

probing the neural mechanisms of cognitive deficits under long COVID conditions.

## Data availability statement

The original contributions presented in the study are included in the article/[Supplementary material](#), further inquiries can be directed to the corresponding authors.

## Ethics statement

The animal study was reviewed and approved by Institutional Animal Ethics Committee (IAEC), IISER Pune.

## Author contributions

NA and SG conceptualized the study. NA supervised all aspects of behavioral phenotyping and morphological analysis. SG supervised all aspects of knockout generation. NA carried out the experimental design. SM, DS, and AS performed behavioral, immunohistochemistry and microscopy experiments and analyzed the data. PS, SDM, and KS performed behavioral experiments and analyzed the data. MS performed knockout generation. SDM performed western blotting experiments. NA and SM wrote the manuscript with comments from others. All authors contributed to the article and approved the submitted version.

## Funding

This work was supported by the DBT/Wellcome Trust India Alliance intermediate grant (IA/I/14/1/501306 to NA), DST-Cognitive Science Research Initiative, Government of India (DST/CSRI/2017/271 to NA), JC Bose Fellowship from the Science and Engineering Research Board, Government of India (JCB/2019/000013 to SG), CSIR Fellowship, Government of India (SM and SDM) and UGC Fellowship, Government of India (KS) Part of the work was carried at the National

Facility for Gene Function in Health and Disease (NFGFHD) at IISER Pune, supported by a grant from the Department of Biotechnology, Government of India (BT/INF/22/SP17358/2016).

## Acknowledgments

The authors thank Laboratory of Neural Circuits and Behavior (LNCB) members for fruitful discussions. The authors also thank staff of National Facility for Gene Function in Health and Disease (NFGFHD) and IISER Biology- Leica microscopy facility for the technical support. This work was carried as part of the contribution of our Institute to the aims and output of the International Mouse Phenotyping Consortium (IMPC. [www.mousephenotype.org](http://www.mousephenotype.org)).

## Conflict of interest

The authors declare that the research was conducted in the absence of any commercial or financial relationships that could be construed as a potential conflict of interest.

## Publisher's note

All claims expressed in this article are solely those of the authors and do not necessarily represent those of their affiliated organizations, or those of the publisher, the editors and the reviewers. Any product that may be evaluated in this article, or claim that may be made by its manufacturer, is not guaranteed or endorsed by the publisher.

## Supplementary material

The Supplementary material for this article can be found online at: <https://www.frontiersin.org/articles/10.3389/fnins.2023.1180868/full#supplementary-material>

## References

- Abraham, N. M., Egger, V., Shimshek, D. R., Renden, R., Fukunaga, I., Sprengel, R., et al. (2010). Synaptic inhibition in the olfactory bulb accelerates odor discrimination in mice. *Neuron* 65, 399–411. doi: 10.1016/j.neuron.2010.01.009
- Abraham, N. M., Spors, H., Carleton, A., Margrie, T. W., Kuner, T., and Schaefer, A. T. (2004). Maintaining accuracy at the expense of speed: stimulus similarity defines odor discrimination time in mice. *Neuron* 44, 865–876. doi: 10.1016/j.neuron.2004.11.017
- Abraham, N. M., Vincis, R., Lagier, S., Rodriguez, I., and Carleton, A. (2014). Long term functional plasticity of sensory inputs mediated by olfactory learning. *Elife* 3:e02109. doi: 10.7554/eLife.02109
- Alenina, N., and Bader, M. (2019). ACE2 in brain physiology and pathophysiology: evidence from transgenic animal models. *Neurochem. Res.* 44, 1323–1329. doi: 10.1007/s11064-018-2679-4
- Barresi, M., Ciurleo, R., Giacoppo, S., Foti Cuzzola, V., Celi, D., Bramanti, P., et al. (2012). Evaluation of olfactory dysfunction in neurodegenerative diseases. *J. Neurol. Sci.* 323, 16–24. doi: 10.1016/j.jns.2012.08.028
- Bayat, A.-H., Azimi, H., Moghaddam, M., Ebrahimi, V., Fathi, M., Vakili, K., et al. (2022). COVID-19 causes neuronal degeneration and reduces neurogenesis in human hippocampus. *Apoptosis* 27, 852–868. doi: 10.1007/s10495-022-01754-9
- Belovicova, K., Bogi, E., Csatosova, K., and Dubovicky, M. (2017). Animal tests for anxiety-like and depression-like behavior in rats. *Interdiscip. Toxicol.* 10, 40–43. doi: 10.1515/intox-2017-0006
- Bhattacharjee, A. S., Joshi, S. V., Naik, S., Sangle, S., and Abraham, N. M. (2020). Quantitative assessment of olfactory dysfunction accurately detects asymptomatic COVID-19 carriers. *EClinicalMedicine* 28:100575. doi: 10.1016/j.eclinm.2020.100575
- Bhattacharjee, A. S., Konakamchi, S., Turaev, D., Vincis, R., Nunes, D., Dingankar, A. A., et al. (2019). Similarity and strength of glomerular odor representations define a neural metric of sniff-invariant discrimination time. *Cell Rep.* 28, 2966–2978.e5. doi: 10.1016/j.celrep.2019.08.015
- Bhowmik, R., Pardasani, M., Mahajan, S., Magar, R., Joshi, S. V., Nair, G. A., et al. (2023). Persistent olfactory learning deficits during and post-COVID-19 infection. *Curr. Res. Neurobiol.* 4:100081. doi: 10.1016/j.crneur.2023.100081
- Bilinska, K., Jakubowska, P., Von Bartheld, C. S., and Butowt, R. (2020). Expression of the SARS-CoV-2 entry proteins, ACE2 and TMPRSS2, in cells of the olfactory epithelium: identification of cell types and trends with age. *ACS Chem. Neurosci.* 11, 1555–1562. doi: 10.1021/acscchemneuro.0c00210
- Boldrini, M., Canoll, P. D., and Klein, R. S. (2021). How COVID-19 affects the brain. *JAMA Psychiat.* 78, 682–683. doi: 10.1001/jamapsychiatry.2021.0500



- Brann, D. H., Tsukahara, T., Weinreb, C., Lipovsek, M., Van den Berge, K., Gong, B., et al. (2020). Non-neuronal expression of SARS-CoV-2 entry genes in the olfactory system suggests mechanisms underlying COVID-19-associated anosmia. *Sci. Adv.* 6:eabc5801. doi: 10.1126/sciadv.abc5801
- Buck, L. B. (2000). The molecular architecture of odor and pheromone sensing in mammals. *Cells* 100, 611–618. doi: 10.1016/S0092-8674(00)80698-4
- Butowt, R., and Bilinska, K. (2020). SARS-CoV-2: olfaction, brain infection, and the urgent need for clinical samples allowing earlier virus detection. *ACS Chem. Neurosci.* 11, 1200–1203. doi: 10.1021/acscchemneuro.0c00172
- Cantuti-Castelvetri, L., Ojha, R., Pedro, L. D., Djannatian, M., Franz, J., Kuivanen, S., et al. (2020). Neuropilin-1 facilitates SARS-CoV-2 cell entry and infectivity. *Science* 370, 856–860. doi: 10.1126/science.abd2985
- Capecchi, M. R. (2005). Gene targeting in mice: functional analysis of the mammalian genome for the twenty-first century. *Nat. Rev. Genet.* 6, 507–512. doi: 10.1038/nrg1619
- Casagrande, M., Fitzek, A., Spitzer, M. S., Püschel, K., Glatzel, M., Krasemann, S., et al. (2021). Presence of SARS-CoV-2 RNA in the cornea of Viremic patients with COVID-19. *JAMA Ophthalmol.* 139, 383–388. doi: 10.1001/jamaophthalmol.2020.6339
- Cooper, K. W., Brann, D. H., Farruggia, M. C., Bhutani, S., Pellegrino, R., Tsukahara, T., et al. (2020). COVID-19 and the chemical senses: supporting players take center stage. *Neuron* 107, 219–233. doi: 10.1016/j.neuron.2020.06.032
- Costanzo, R. M. (2000). Rewiring the olfactory bulb: changes in odor maps following recovery from nerve transection. *Chem. Senses* 25, 199–205. doi: 10.1093/chemse/25.2.199
- Crackower, M. A., Sarao, R., Oudit, G. Y., Yagil, C., Kozieradzki, I., Scanga, S. E., et al. (2002). Angiotensin-converting enzyme 2 is an essential regulator of heart function. *Nature* 417, 822–828. doi: 10.1038/nature00786
- Crews, L., and Hunter, D. (1994). Neurogenesis in the olfactory epithelium. *Perspect. Dev. Neurobiol.* 2, 151–161.
- De Melo, G. D., Lazarini, F., Levallois, S., Hautefort, C., Michel, V., Larrous, F., et al. (2021). COVID-19-related anosmia is associated with viral persistence and inflammation in human olfactory epithelium and brain infection in hamsters. *Sci. Transl. Med.* 13:eabf8396. doi: 10.1126/scitranslmed.abf8396
- Donoghue, M., Hsieh, F., Baronas, E., Godbout, K., Gosselin, M., Stagliano, N., et al. (2000). A novel angiotensin-converting enzyme-related carboxypeptidase (ACE2) converts angiotensin I to angiotensin 1–9. *Circ. Res.* 87, E1–E9. doi: 10.1161/01.res.87.5.e1
- Doty, R. L. (2012). Olfactory dysfunction in Parkinson disease. *Nat. Rev. Neurol.* 8, 329–339. doi: 10.1038/nrneurol.2012.80
- Douaud, G., Lee, S., Alfaro-Almagro, F., Arthofer, C., Wang, C., McCarthy, P., et al. (2022). SARS-CoV-2 is associated with changes in brain structure in UK biobank. *Nature* 604, 697–707. doi: 10.1038/s41586-022-04569-5
- Du, Y., Zhao, W., Huang, S., Huang, Y., Chen, Y., Zhang, H., et al. (2023). Two-year follow-up of brain structural changes in patients who recovered from COVID-19: A prospective study. *Psychiatry Res.* 319, 114969. doi: 10.1016/j.psychres.2022.114969
- Evans, C. E., Miners, J. S., Piva, G., Willis, C. L., Heard, D. M., Kidd, E. J., et al. (2020). ACE2 activation protects against cognitive decline and reduces amyloid pathology in the Tg2576 mouse model of Alzheimer's disease. *Acta Neuropathol.* 139, 485–502. doi: 10.1007/s00401-019-02098-6
- Fleming, S. M., Tetreault, N. A., Mulligan, C. K., Hutson, C. B., Masliah, E., and Chesselet, M.-F. (2008). Olfactory deficits in mice overexpressing human wildtype alpha-synuclein. *Eur. J. Neurosci.* 28, 247–256. doi: 10.1111/j.1460-9568.2008.06346.x
- Fodoulan, L., Tuberosa, J., Rossier, D., Boillat, M., Kan, C., Pauli, V., et al. (2020). SARS-CoV-2 receptors and entry genes are expressed in the human olfactory neuroepithelium and brain 23:101839. doi: 10.1016/j.isci.2020.101839
- Fullard, M. E., Morley, J. F., and Duda, J. E. (2017). Olfactory dysfunction as an early biomarker in Parkinson's disease. *Neurosci. Bull.* 33, 515–525. doi: 10.1007/s12264-017-0170-x
- Glowacka, I., Bertram, S., Müller, M. A., Allen, P., Soilleux, E., Pfefferle, S., et al. (2011). Evidence that TMPRSS2 activates the severe acute respiratory syndrome coronavirus spike protein for membrane fusion and reduces viral control by the humoral immune response. *J. Virol.* 85, 4122–4134. doi: 10.1128/JVI.02232-10
- Hamming, I., Timens, W., Bulthuis, M. L. C., Lely, A. T., Navis, G. J., and van Goor, H. (2004). Tissue distribution of ACE2 protein, the functional receptor for SARS coronavirus. A first step in understanding SARS pathogenesis. *J. Pathol.* 203, 631–637. doi: 10.1002/path.1570
- Hampshire, A., Trender, W., Chamberlain, S. R., Jolly, A. E., Grant, J. E., Patrick, F., et al. (2021). Cognitive deficits in people who have recovered from COVID-19. *EClinicalMedicine* 39:101044. doi: 10.1016/j.eclinm.2021.101044
- Harms, D. W., Quadros, R. M., Seruggia, D., Ohtsuka, M., Takahashi, G., Montoliu, L., et al. (2014). Mouse genome editing using the CRISPR/Cas system. *Curr. Protoc. Hum. Genet.* 83, 15.7.1–15.7.27. doi: 10.1002/0471142905.hg1507s83
- Hoffmann, M., Kleine-Weber, H., Schroeder, S., Krüger, N., Herrler, T., Erichsen, S., et al. (2020). SARS-CoV-2 cell entry depends on ACE2 and TMPRSS2 and is blocked by a clinically proven protease inhibitor. *Cells* 181, 271–280.e8. doi: 10.1016/j.cell.2020.02.052
- Huang, X., Hussain, B., and Chang, J. (2021). Peripheral inflammation and blood-brain barrier disruption: effects and mechanisms. *CNS Neurosci. Ther.* 27, 36–47. doi: 10.1111/cns.13569
- Huang, N., Pérez, P., Kato, T., Mikami, Y., Okuda, K., Gilmore, R. C., et al. (2021). SARS-CoV-2 infection of the oral cavity and saliva. *Nat. Med.* 27, 892–903. doi: 10.1038/s41591-021-01296-8
- Hugon, J., Msika, E.-F., Queneau, M., Farid, K., and Paquet, C. (2022). Long COVID: cognitive complaints (brain fog) and dysfunction of the cingulate cortex. *J. Neurol.* 269, 44–46. doi: 10.1007/s00415-021-10655-x
- Iravani, B., Arshamian, A., and Lundström, J. N. (2022). Loss of olfactory sensitivity is an early and reliable marker for COVID-19. *Chem. Senses* 47:bjac022. doi: 10.1093/chemse/bjac022
- Jackson, C. B., Farzan, M., Chen, B., and Choe, H. (2022). Mechanisms of SARS-CoV-2 entry into cells. *Nat. Rev. Mol. Cell Biol.* 23, 3–20. doi: 10.1038/s41580-021-00418-x
- Jia, H., Yue, X., and Lazartigues, E. (2020). ACE2 mouse models: a toolbox for cardiovascular and pulmonary research. *Nat. Commun.* 11:5165. doi: 10.1038/s41467-020-18880-0
- John, J. A. S., and Key, B. (2003). Axon mis-targeting in the olfactory bulb during regeneration of olfactory neuroepithelium. *Chem. Senses* 28, 773–779. doi: 10.1093/chemse/bjg068
- Kang, Y., Chu, C., Wang, F., and Niu, Y. (2019). CRISPR/Cas9-mediated genome editing in nonhuman primates. *Dis. Model. Mech.* 12:dmm039982. doi: 10.1242/dmm.039982
- Kay, L. M. (2022). COVID-19 and olfactory dysfunction: a looming wave of dementia? *J. Neurophysiol.* 128, 436–444. doi: 10.1152/jn.00255.2022
- Khan, M., Yoo, S.-J., Clijsters, M., Backaert, W., Vanstapel, A., Speleman, K., et al. (2021). Visualizing in deceased COVID-19 patients how SARS-CoV-2 attacks the respiratory and olfactory mucosae but spares the olfactory bulb. *Cells* 184, 5932–5949.e15. doi: 10.1016/j.cell.2021.10.027
- Klempin, F., Mosienko, V., Matthes, S., Villela, D. C., Todiras, M., Penninger, J. M., et al. (2018). Depletion of angiotensin-converting enzyme 2 reduces brain serotonin and impairs the running-induced neurogenic response. *Cell. Mol. Life Sci.* 75, 3625–3634. doi: 10.1007/s00018-018-2815-y
- Klingenstein, M., Klingenstein, S., Neckel, P. H., Mack, A. F., Wagner, A. P., Kleger, A., et al. (2020). Evidence of SARS-CoV2 entry protein ACE2 in the human nose and olfactory bulb. *Cells Tissues Organs* 209, 155–164. doi: 10.1159/000513040
- Kyrou, I., Randevara, H. S., Spandidos, D. A., and Karteris, E. (2021). Not only ACE2—the quest for additional host cell mediators of SARS-CoV-2 infection: Neuropilin-1 (NRP1) as a novel SARS-CoV-2 host cell entry mediator implicated in COVID-19. *Signal Transduct. Target. Ther.* 6:21. doi: 10.1038/s41392-020-00460-9
- Lamontagne, S. J., Winters, M. F., Pizzagalli, D. A., and Olmstead, M. C. (2021). Post-acute sequelae of COVID-19: evidence of mood & cognitive impairment. *Brain Behav. Immun. Health* 17:100347. doi: 10.1016/j.bbih.2021.100347
- Lechien, J. R., Radulesco, T., Calvo-Henriquez, C., Chiesa-Estomba, C. M., Hans, S., Barillari, M. R., et al. (2021). ACE2 & TMPRSS2 expressions in Head & Neck Tissues: A systematic review. *Head Neck Pathol.* 15, 225–235. doi: 10.1007/s12105-020-01212-5
- Lehmkuhl, A. M., Dirr, E. R., and Fleming, S. M. (2014). Olfactory assays for mouse models of neurodegenerative disease. *JoVE* 90:e51804. doi: 10.3791/51804
- Li, W.-S., Chan, L.-L., Chao, Y.-X., and Tan, E.-K. (2020). Parkinson's disease following COVID-19: causal link or chance occurrence? *J. Transl. Med.* 18:493. doi: 10.1186/s12967-020-02670-9
- Mahammedi, A., Ramos, A., Bargalló, N., Gaskill, M., Kapur, S., Saba, L., et al. (2021). Brain and lung imaging correlation in patients with COVID-19: could the severity of lung disease reflect the prevalence of acute abnormalities on neuroimaging? A global multicenter observational study. *AJNR Am. J. Neuroradiol.* 42, 1008–1016. doi: 10.3174/ajnr.A7072
- Mainland, J. D., Li, Y. R., Zhou, T., Liu, W. L. L., and Matsunami, H. (2015). Human olfactory receptor responses to odorants. *Sci. Data* 2:150002. doi: 10.1038/sdata.2015.2
- Manchia, M., Gathier, A. W., Yapici-Eser, H., Schmidt, M. V., de Quervain, D., van Amelsvoort, T., et al. (2022). The impact of the prolonged COVID-19 pandemic on stress resilience and mental health: a critical review across waves. *Eur. Neuropsychopharmacol.* 55, 22–83. doi: 10.1016/j.euroneuro.2021.10.864
- Marin, C., Vilas, D., Langdon, C., Alobid, I., López-Chacón, M., Haehner, A., et al. (2018). Olfactory dysfunction in neurodegenerative diseases. *Curr. Allergy Asthma Rep.* 18:42. doi: 10.1007/s11882-018-0796-4
- McGann, J. P. (2017). Poor human olfaction is a 19th-century myth. *Science* 356:eaam7263. doi: 10.1126/science.aam7263
- Meinhardt, J., Radke, J., Dittmayer, C., Franz, J., Thomas, C., Mothes, R., et al. (2021). Olfactory transnucosal SARS-CoV-2 invasion as a port of central nervous system entry in individuals with COVID-19. *Nat. Neurosci.* 24, 168–175. doi: 10.1038/s41593-020-00758-5
- Merello, M., Bhatia, K. P., and Obeso, J. A. (2021). SARS-CoV-2 and the risk of Parkinson's disease: facts and fantasy. *Lancet Neurol.* 20, 94–95. doi: 10.1016/S1474-4422(20)30442-7

- Nishizono, H., Yasuda, R., and Laviv, T. (2020). Methodologies and challenges for CRISPR/Cas9 mediated genome editing of the mammalian brain. *Front. Genome Ed.* 2:602970. doi: 10.3389/fgeed.2020.602970
- Pardasani, M., and Abraham, N. M. (2022). "Neurotropic SARS-CoV-2: causalities and realities" in *COVID-19 pandemic, mental health and neuroscience - new scenarios for understanding and treatment*. eds. P. D. S. Palermo and P. B. Olivier (Rijeka: IntechOpen)
- Pardasani, M., Marathe, S. D., Purnapatre, M. M., Dalvi, U., and Abraham, N. M. (2021). Multimodal learning of pheromone locations. *FASEB J.* 35:e21836. doi: 10.1096/fj.202100167R
- Pascoal, P. M., Carvalho, J., Raposo, C. F., Almeida, J., and Beato, A. F. (2021). The impact of COVID-19 on sexual health: A preliminary framework based on a qualitative study with clinical sexologists. *Sex. Med.* 9:100299. doi: 10.1016/j.esxm.2020.100299
- Potter, S. M., Zheng, C., Koos, D. S., Feinstein, P., Fraser, S. E., and Mombaerts, P. (2001). Structure and emergence of specific olfactory glomeruli in the mouse. *J. Neurosci.* 21, 9713–9723. doi: 10.1523/JNEUROSCI.21-24-09713.2001
- Puelles, V. G., Lütgehetmann, M., Lindenmeyer, M. T., Sperhake, J. P., Wong, M. N., Allweiss, L., et al. (2020). Multiorgan and renal tropism of SARS-CoV-2. *N. Engl. J. Med.* 383, 590–592. doi: 10.1056/NEJMc2011400
- Shang, J., Wan, Y., Luo, C., Ye, G., Geng, Q., Auerbach, A., et al. (2020). Cell entry mechanisms of SARS-CoV-2. *Proc. Natl. Acad. Sci. U. S. A.* 117, 11727–11734. doi: 10.1073/pnas.2003138117
- Shao, Y., Guan, Y., Wang, L., Qiu, Z., Liu, M., Chen, Y., et al. (2014). CRISPR/Cas-mediated genome editing in the rat via direct injection of one-cell embryos. *Nat. Protoc.* 9, 2493–2512. doi: 10.1038/nprot.2014.171
- Stephan, M., Volkman, P., and Rossner, M. J. (2022). Assessing behavior and cognition in rodents, nonhuman primates, and humans: Where are the limits of translation? *Dialogues Clin. Neurosci.* 21, 249–259. doi: 10.31887/DCNS.2019.21.3/mrossner
- Sulzer, D., Antonini, A., Leta, V., Nordvig, A., Smeyne, R. J., Goldman, J. E., et al. (2020). COVID-19 and possible links with Parkinson's disease and parkinsonism: from bench to bedside. *NPJ Parkinsons Dis.* 6:18. doi: 10.1038/s41531-020-00123-0
- Sungnak, W., Huang, N., Bécavin, C., Berg, M., Queen, R., Litvinukova, M., et al. (2020). SARS-CoV-2 entry factors are highly expressed in nasal epithelial cells together with innate immune genes. *Nat. Med.* 26, 681–687. doi: 10.1038/s41591-020-0868-6
- Taniguchi, H., He, M., Wu, P., Kim, S., Paik, R., Sugino, K., et al. (2011). A resource of Cre driver lines for genetic targeting of GABAergic neurons in cerebral cortex. *Neuron* 71, 995–1013. doi: 10.1016/j.neuron.2011.07.026
- Tillerson, J. L., Caudle, W. M., Parent, J. M., Gong, C., Schallert, T., and Miller, G. W. (2006). Olfactory discrimination deficits in mice lacking the dopamine transporter or the D2 dopamine receptor. *Behav. Brain Res.* 172, 97–105. doi: 10.1016/j.bbr.2006.04.025
- Verdecchia, P., Cavallini, C., Spanevello, A., and Angeli, F. (2020). The pivotal link between ACE2 deficiency and SARS-CoV-2 infection. *Eur. J. Intern. Med.* 76, 14–20. doi: 10.1016/j.ejim.2020.04.037
- Wang, X.-L., Iwanami, J., Min, L.-J., Tsukuda, K., Nakaoka, H., Bai, H.-Y., et al. (2016). Deficiency of angiotensin-converting enzyme 2 causes deterioration of cognitive function. *NPJ Aging Mech. Dis.* 2:16024. doi: 10.1038/npjamd.2016.24
- Whitcroft, K. L., and Hummel, T. (2020). Olfactory dysfunction in COVID-19: diagnosis and management. *JAMA* 323, 2512–2514. doi: 10.1001/jama.2020.8391
- Whittaker, G. R., Daniel, S., and Millet, J. K. (2021). Coronavirus entry: how we arrived at SARS-CoV-2. *Curr. Opin. Virol.* 47, 113–120. doi: 10.1016/j.coviro.2021.02.006
- WHO. (2022). *COVID-19 pandemic triggers 25% increase in prevalence of anxiety and depression worldwide*. Geneva: World Health Organization.
- Yang, H., Wang, H., Shivalila, C. S., Cheng, A. W., Shi, L., and Jaenisch, R. (2013). One-step generation of mice carrying reporter and conditional alleles by CRISPR/Cas-mediated genome engineering. *Cells* 154, 1370–1379. doi: 10.1016/j.cell.2013.08.022
- Yuksel, B., and Ozgor, F. (2020). Effect of the COVID-19 pandemic on female sexual behavior. *Int. J. Gynaecol. Obstet.* 150, 98–102. doi: 10.1002/ijgo.13193
- Zhou, L., Xu, Z., Castiglione, G. M., Soiberman, U. S., Eberhart, C. G., and Duh, E. J. (2020). ACE2 and TMPRSS2 are expressed on the human ocular surface, suggesting susceptibility to SARS-CoV-2 infection. *Ocul. Surf.* 18, 537–544. doi: 10.1016/j.jtos.2020.06.007